

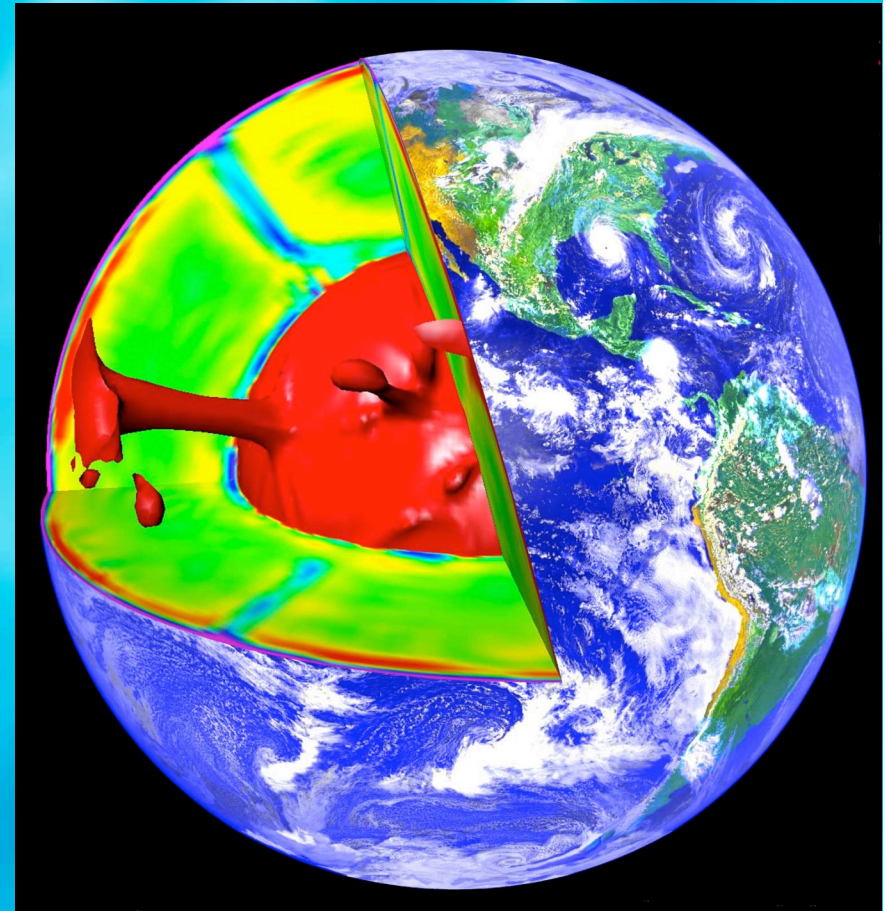
# 3D Spherical Mantle Convection Calculations using the Yin-Yang grid

**Paul Tackley**

**ETHZ Institut für Geophysik**

(contributions from T.  
Nakagawa (Kyushu U.)

J. Hernlund (UBC), F.  
Deschamps, J. Connolly)



# 11<sup>th</sup> International Workshop on Modeling of Mantle Convection and Lithospheric Dynamics

June 28 - July 3, 2009, Braunwald, Switzerland

[Home](#)

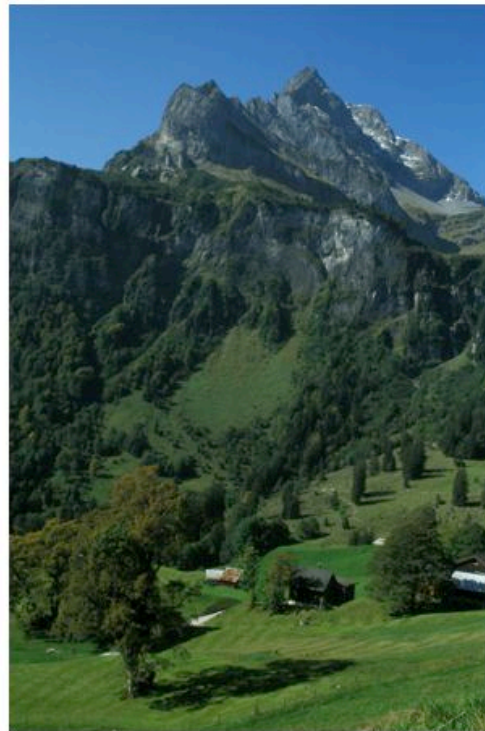
[Program and invited presentations](#)

[Participants, abstracts and posters](#)

[Support](#)

[Practical informations](#)

[Send an E-mail](#)



## Local organizing committee (ETH Zurich):

Paul Tackley (Geophysical Fluid Dynamics)  
Taras Gerya (Geophysical Fluid Dynamics)  
Boris Kaus (Geophysical Fluid Dynamics)  
Frédéric Deschamps (Geophysical Fluid Dynamics)  
Lapo Boschi (Seismology and Geodynamics)  
Stefan Schmalholz (Structural Geology and Tectonics)

---

## Scientific Committee

Stéphane Labrosse (ENS Lyon) Allen McNamara (Univ. Arizona) Louis Moresi (Monash Univ.)  
Stephan Sobolev (GFZ Postdam) Trond Torsvik (NGU Trondheim)

## Purpose & goals

This workshop is the next in a series of successful workshops held in various locations throughout Europe approximately every 2 years, since 1989 (the three previous ones have been held in [Carry-le-Rouet \(2007\)](#), [Erice \(2005\)](#), [Hruba Skala \(2003\)](#)), and it is generally regarded as the main European conference in geodynamics. The main goals of this workshop are:

- to provide a forum for in-depth discussion on scientific and technical issues in geodynamic modelling, and integration with other related fields,
- to introduce students and postdocs to the breadth of current geodynamic research, in an informal setting
- to foster interdisciplinary and international collaboration.

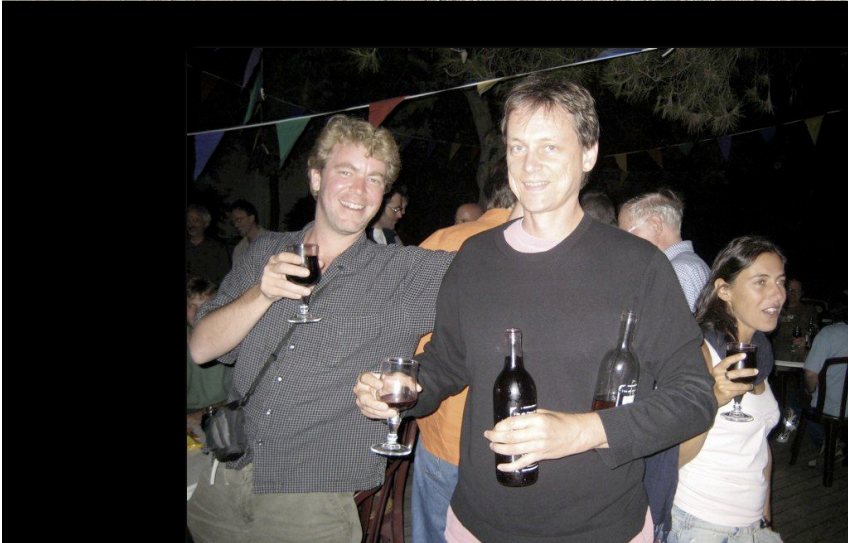
The workshop has a five-day program with oral presentation provided solely by invited keynote speakers, and a possibility for poster presentations for all other participants. Two types of lectures are planned:

- talks on the state-of-the-art research in geodynamics and directly neighbouring research fields
- educational, tutorial-type talks to give scientific and technical background information for a specific research area.

Apart from lectures and poster sessions, hands-on mini workshops on numerical modelling, and break-out or discussion sessions on, for example, modelling benchmarks will be organized.

<http://www.gfd.ethz.ch/~braunwald2009/index.html>

# Carry 2007



# Braunwald 2009



# Outline

- ⦿ Background
- ⦿ Technical details
- ⦿ Examples

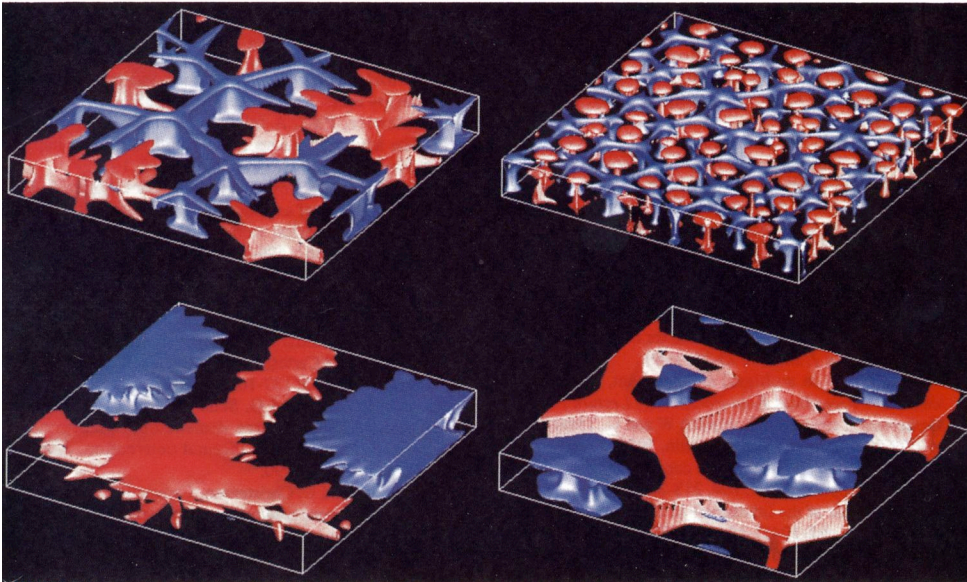
# Stag3D: 1992-

1998 AGU monograph

1993 GRL

Tackley: 3-D Convection with Temperature-Dependent Viscosity

2189



Compressible TALA

3D cartesian  
2D cartesian, axisymmetric  
or cylindrical

Tackley, 1997

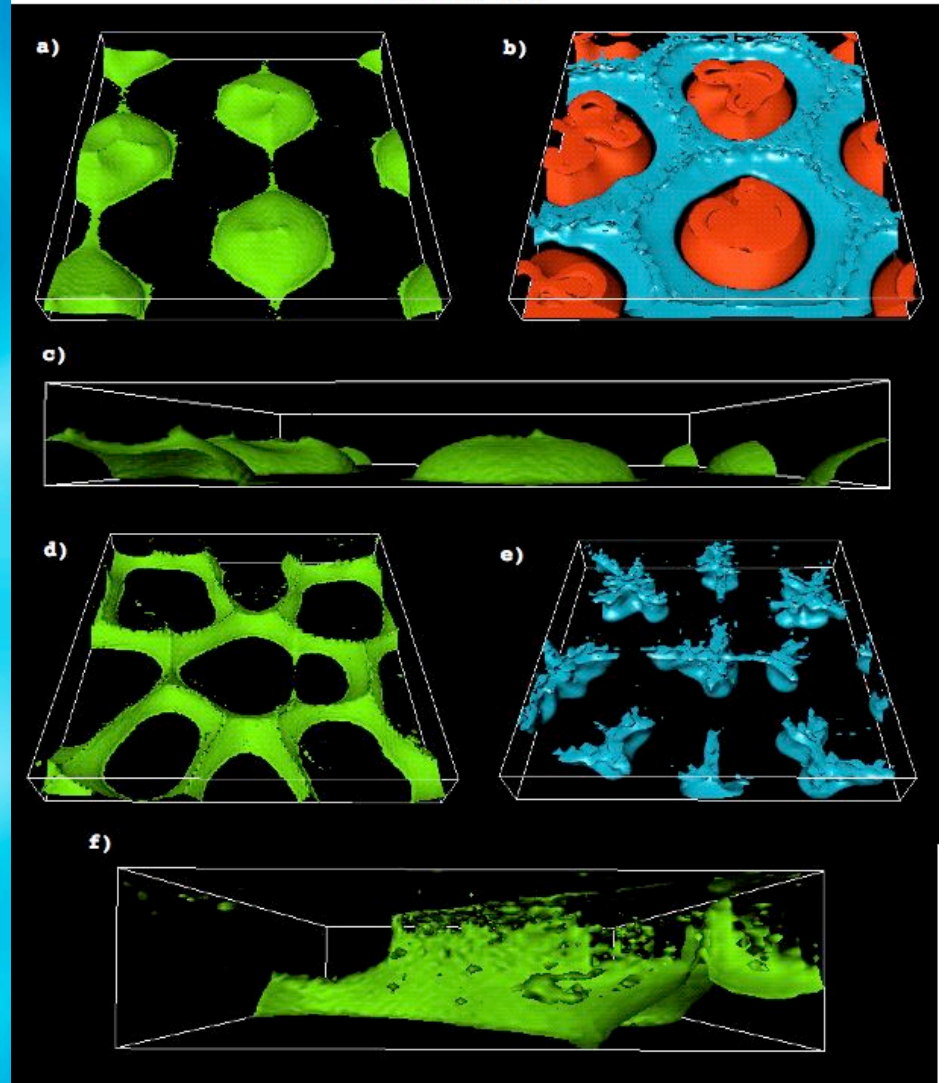
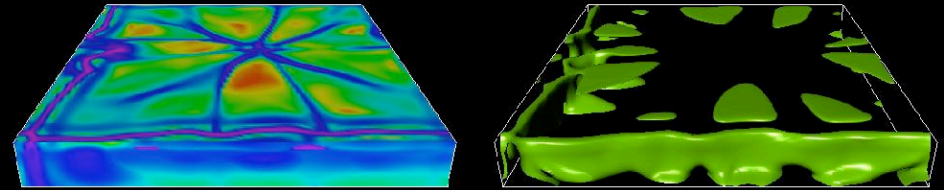


Figure CC

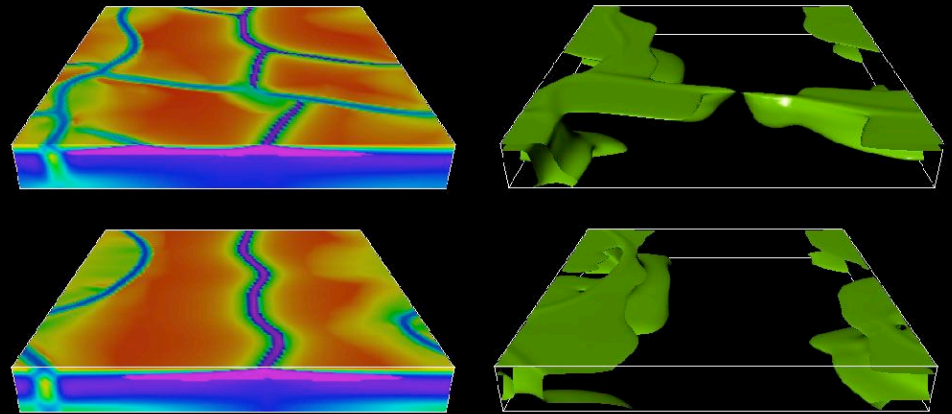
# YIELDING CAN PRODUCE PLATE TECTONICS

## Self-consistent plate tectonics (2000ab)

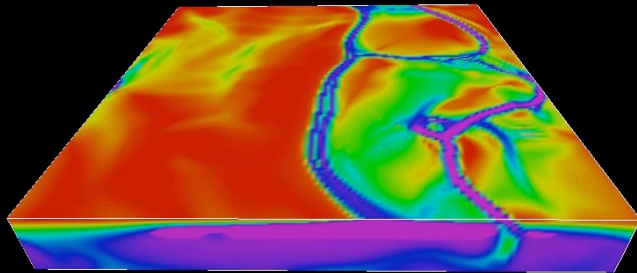
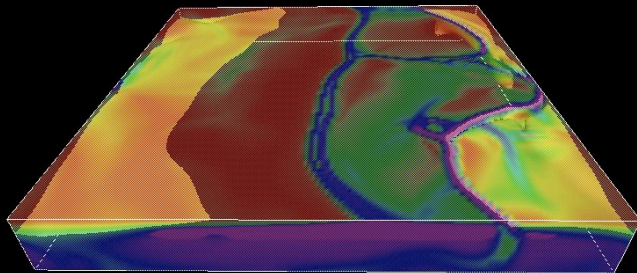
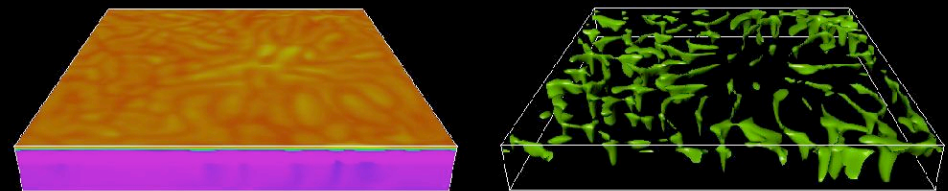
Low yield stress: weak plates, diffuse deformation



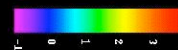
Intermediate yield stress: Good plate tectonics



High yield stress: Immobile lithosphere



viscosity



cold T (downwellings)

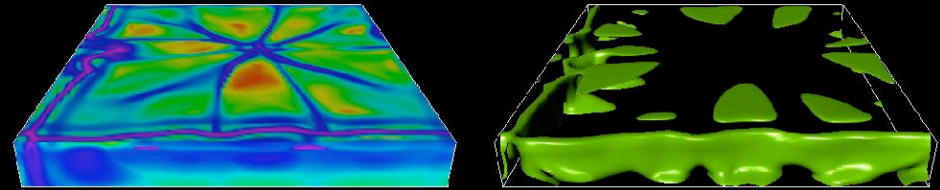
by Paul J. Tackley 2000



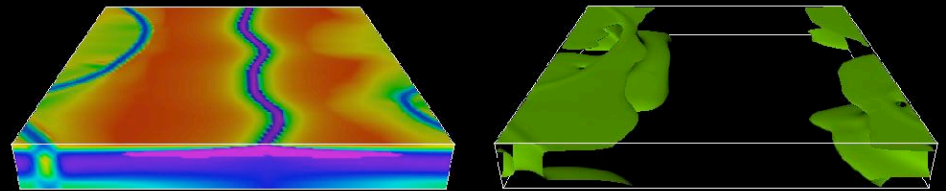
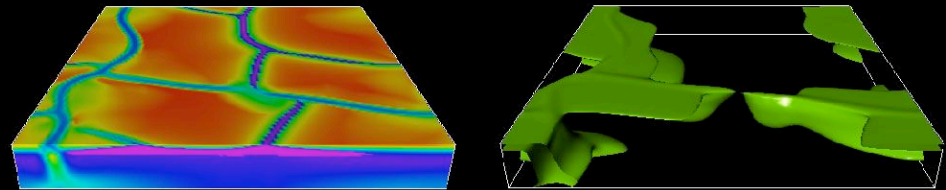
# YIELDING CAN PRODUCE PLATE TECTONICS

## Cartesian: how to make spherical?

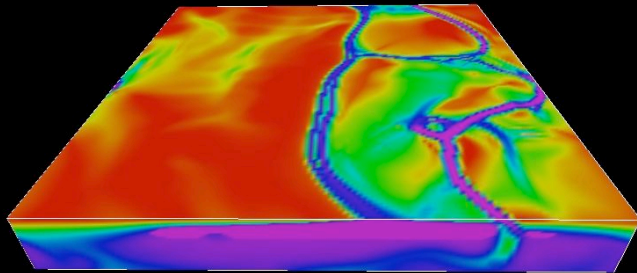
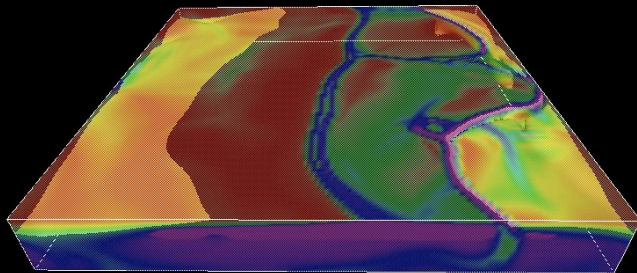
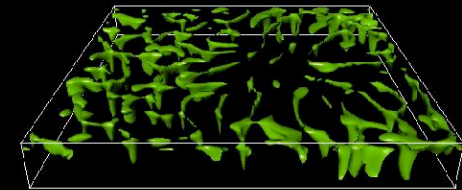
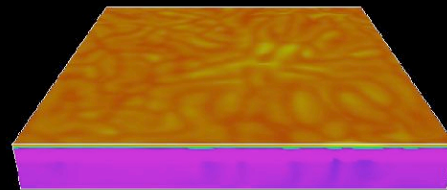
Low yield stress: weak plates, diffuse deformation



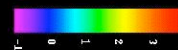
Intermediate yield stress: Good plate tectonics



High yield stress: Immobile lithosphere



viscosity



cold T (downwellings)

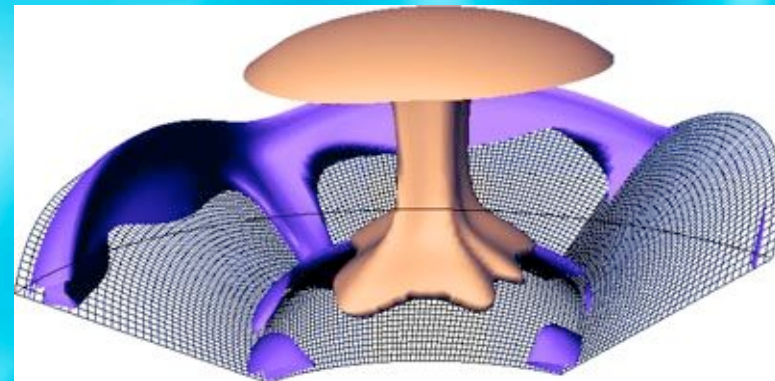
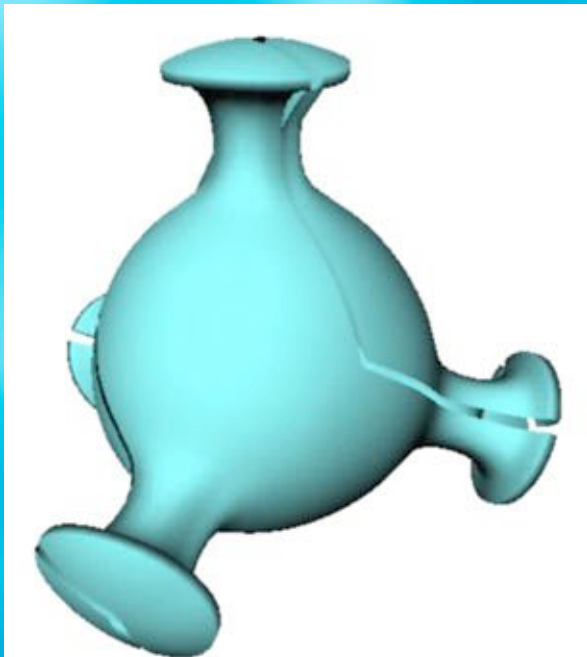
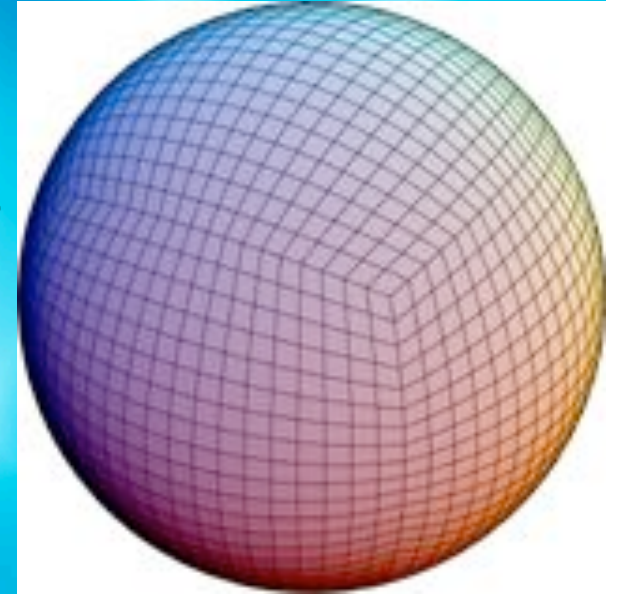
by Paul J. Tackley 2000

# Grid-based spherical codes

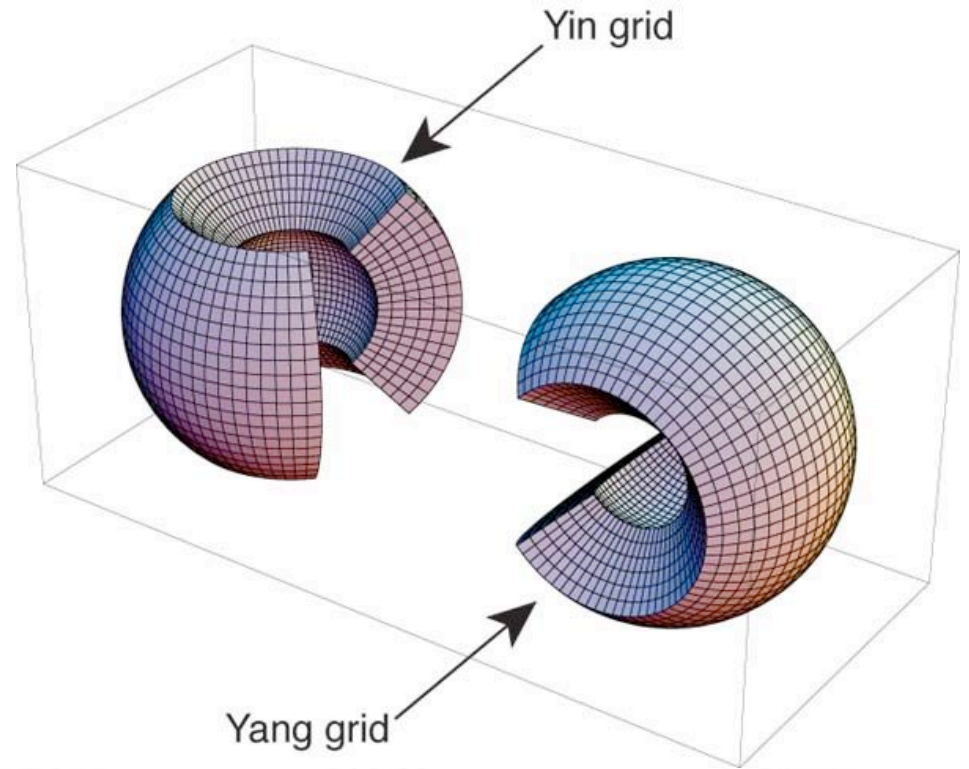
- ⊙ Longitude-latitude mesh: Zebib, Iwase & Honda
  - Finite-difference / finite volume, Gauss-Seidel iterations. Pole problem but possible solution.
- ⊙ Isocahedral mesh: TERRA (Baumgardner)
  - Finite element, multigrid solver
- ⊙ Multiple (12) quadrilateral blocks mesh: CITCOM-S (Zhong/Moresi)
  - Finite element, multigrid solver, non-orthogonal
- ⊙ “Cubed sphere” grid: Grasset, Hernlund, Harder
  - Finite difference, multigrid solver
- ⊙ “Yin-Yang” grid: Yoshida/Kageyama code
  - Finite difference, multigrid solver

# “Cubed sphere” grid

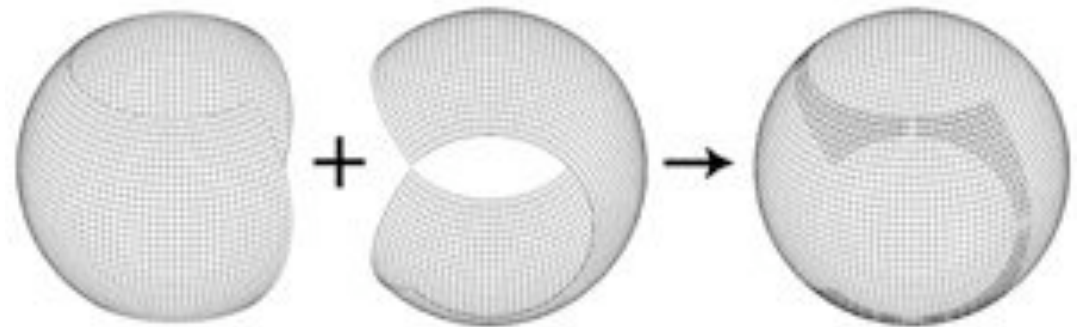
- Cube projected onto sphere then subdivided
- Several possible methods of doing subdivisions
- Typically leads to non-orthogonal grid, leading to complicated equations (FD, FV methods), though Harder has an approximately orthogonal version.
- Example results from Hernlund’s code



# 'Yin-Yang' grid (Kageyama, JAMSTEC ESC)



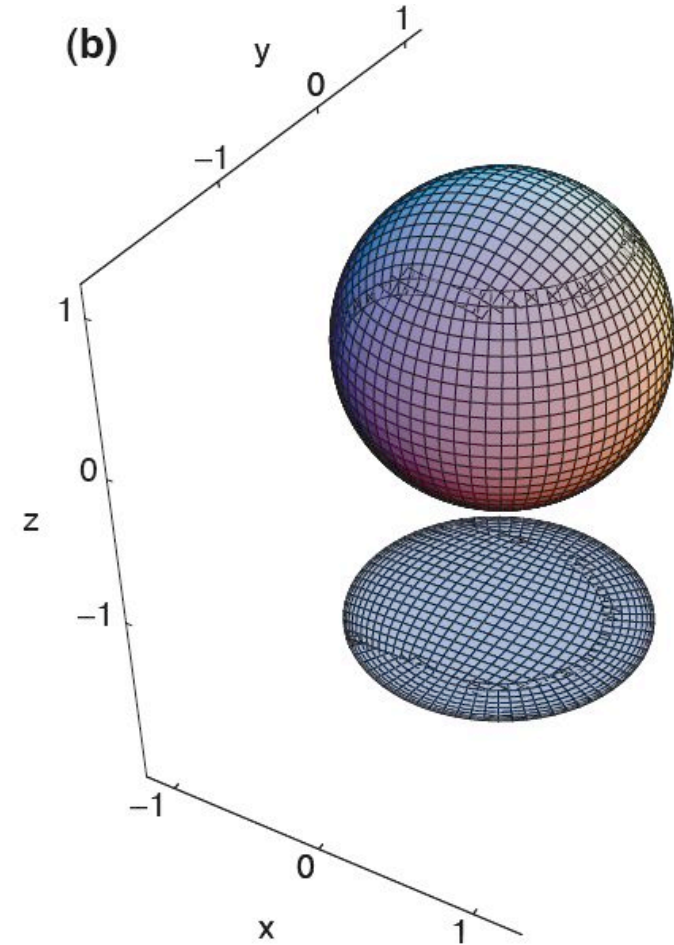
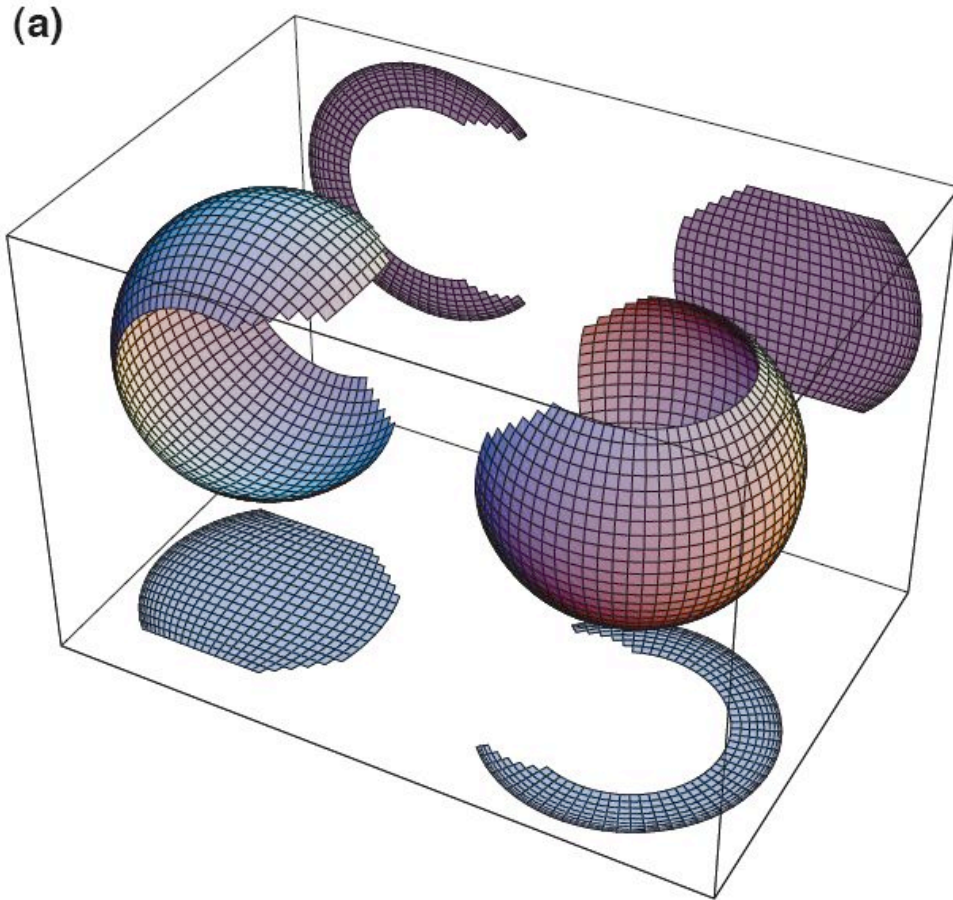
⊙ Orthogonal =>  
simple finite-  
differences  
possible



⊙ Overlapping  
region (6% of  
total)

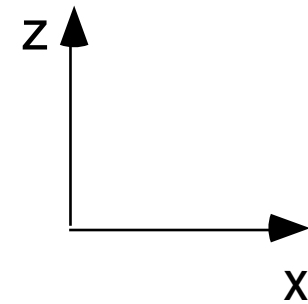
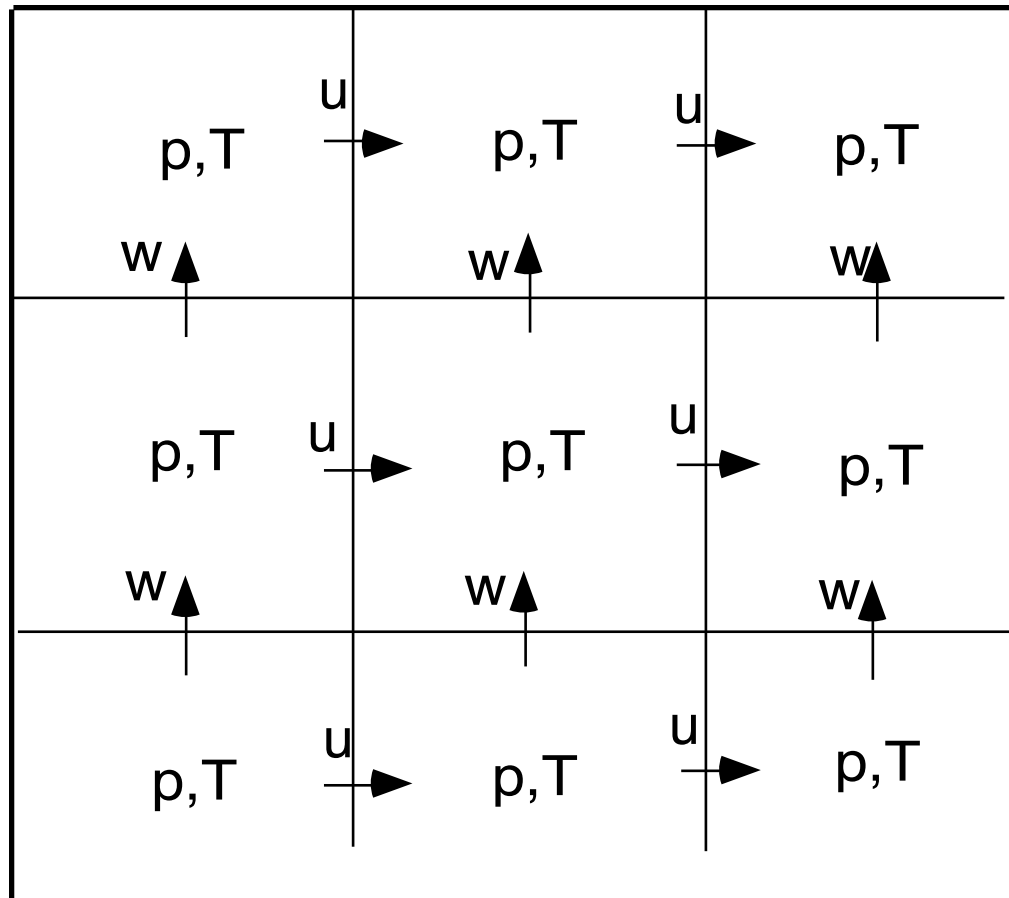


# Minimum overlap YY grid



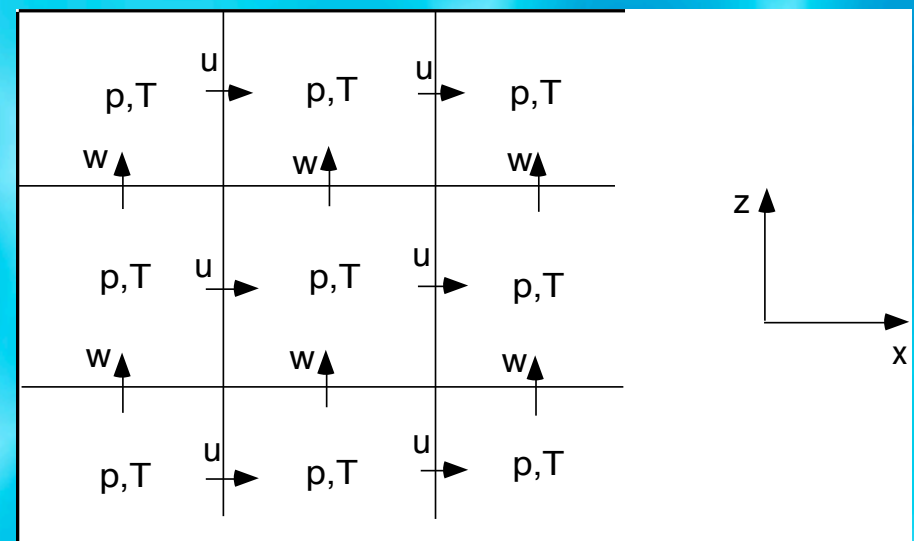
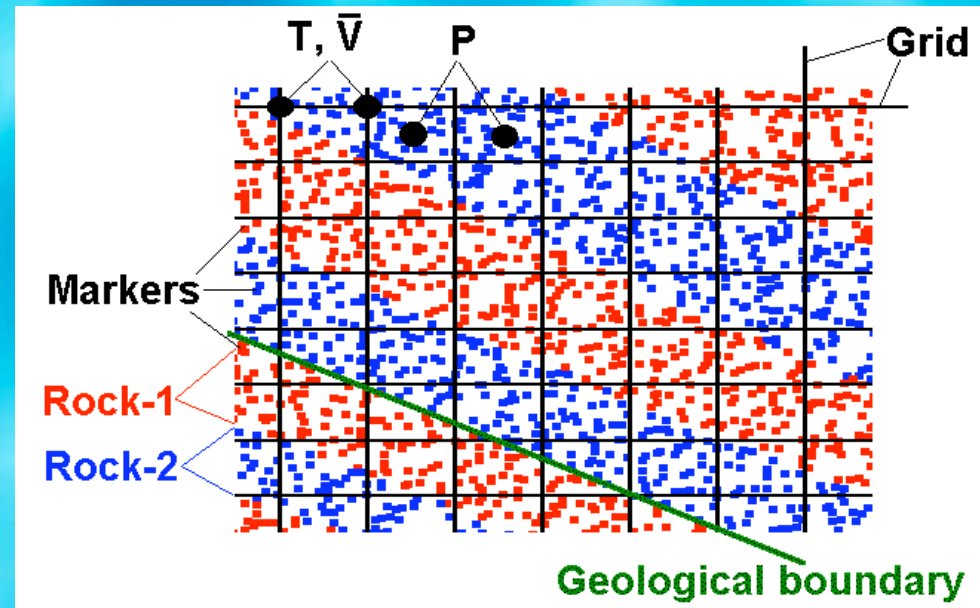
- ⦿ Eliminates differing solutions in overlap
- ⦿ Jagged boundaries of subgrids

# Staggered grid primitive variables



# Compositional treatment uses tracers

- Track composition on Lagrangian tracers
- (Eulerian grid, as before)



# Truncated anelastic equations

Conservation of mass:

$$\nabla \cdot (\rho \underline{v}) = 0 \quad , \quad (1)$$

momentum

$$\underline{\nabla} \cdot \underline{\underline{\sigma}} - \underline{\nabla} p = Ra \cdot \hat{\underline{r}} \cdot \rho(C, r, T) / \Delta \rho_{thermal} \quad (2)$$

and energy

$$\rho C_p \frac{DT}{Dt} = -Di_s \alpha \rho T v_r + \underline{\nabla} \cdot (k \nabla T) + \rho H + \frac{Di_s}{Ra} \underline{\underline{\sigma}} : \underline{\underline{\dot{\epsilon}}} \quad (3)$$

In cases where bulk chemistry is treated the following must also be satisfied:

$$\frac{DC}{Dt} = 0$$



# Spherical stress divergences

$$(\nabla \cdot \underline{\underline{\sigma}})_r = -\frac{\partial p}{\partial r} + \frac{1}{r^2} \frac{\partial}{\partial r} (r^2 \tau_{rr}) + \frac{1}{r \sin \theta} \frac{\partial}{\partial \theta} (\tau_{r\theta} \sin \theta) + \frac{1}{r \sin \theta} \frac{\partial \tau_{r\phi}}{\partial \phi} - \frac{\tau_{\theta\theta} + \tau_{\phi\phi}}{r} \quad (5)$$

$$(\nabla \cdot \underline{\underline{\sigma}})_\theta = -\frac{1}{r} \frac{\partial p}{\partial \theta} + \frac{1}{r^2} \frac{\partial}{\partial r} (r^2 \tau_{r\theta}) + \frac{1}{r \sin \theta} \frac{\partial}{\partial \theta} (\tau_{\theta\theta} \sin \theta) + \frac{1}{r \sin \theta} \frac{\partial \tau_{\phi\theta}}{\partial \phi} + \frac{1}{r} (\tau_{r\theta} - \tau_{\phi\phi} \cot \theta) \quad (6)$$

$$(\nabla \cdot \underline{\underline{\sigma}})_\phi = -\frac{1}{r \sin \theta} \frac{\partial p}{\partial \phi} + \frac{1}{r^2} \frac{\partial}{\partial r} (r^2 \tau_{r\phi}) + \frac{1}{r \sin \theta} \frac{\partial}{\partial \theta} (\tau_{\theta\phi} \sin \theta) + \frac{1}{r \sin \theta} \frac{\partial \tau_{\phi\phi}}{\partial \phi} + \frac{1}{r} (\tau_{r\phi} + \tau_{\theta\phi} \cot \theta) \quad (7)$$

# Iteration procedure (velocity/pressure)

- ⊙ Pointwise (~like Patankar's SIMPLER)
  - Update x-velocities
  - Update y-velocities
  - Update z-velocities
  - Update pressure to reduce  $\text{div.v}$
- ⊙ Cellwise ('pressure coupled')
  - Solve pressure + 6 surrounding v components simultaneously
  - Converges better but slower
  - Not yet implemented in new version

A subtlety occurs in the treatment of normal strain rates (hence normal stresses) when density is spatially varying, i.e., for compressible cases. The divergence of velocity is then non-zero and the expressions for normal strain rate contain a  $-\frac{1}{3}\nabla \cdot \underline{v}$ . If this is calculated literally from the velocities, then instabilities can occur in an iterative solution procedure, because  $\nabla \cdot \underline{v}$  can be incorrectly very high or low during early iterations. Thus, it is better to recognise that:

$$\nabla \cdot (\rho \underline{v}) = 0 = \rho \nabla \cdot \underline{v} + \underline{v} \cdot \nabla \rho \quad \Rightarrow \quad \nabla \cdot \underline{v} = \frac{-\underline{v} \cdot \nabla \rho}{\rho} \quad (8)$$

and use  $\underline{v} \cdot \nabla \rho / \rho$  in the strain rate expressions instead of  $\nabla \cdot \underline{v}$ , because velocities is more reliable than gradients of velocity. This simply appears as an extra term in the calculation of the finite-difference stencils.

# Iterations: details

Velocity correction

$$\delta v_{i-.5jk}^{\theta} = -\alpha_m R_{i-.5jk}^{\theta mom} / \left( \frac{\partial R_{i-.5jk}^{\theta mom}}{\partial v_{i-.5jk}^{\theta}} \right)$$

Pressure correction  
(to reduce divergence)

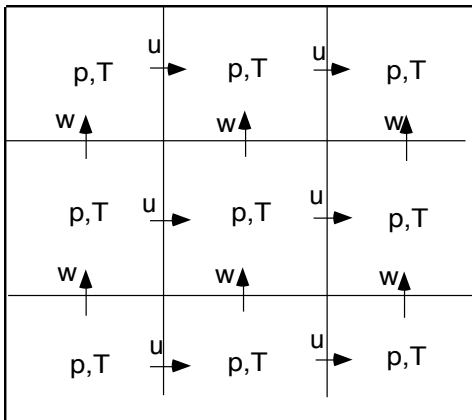
$$\delta P_{ijk} = -\alpha_c R_{ijk}^{cont} / \left( \frac{\partial R_{ijk}^{cont}}{\partial P_{ijk}} \right)$$

Velocity update  
for pressure  
correction

$$\delta v_{i-.5jk}^{\theta} = \left( \delta P_{i-1jk} \left( \frac{\partial R_{i-.5jk}^{\theta mom}}{\partial P_{i-1jk}} \right) + \delta P_{ijk} \left( \frac{\partial R_{i-.5jk}^{\theta mom}}{\partial P_{ijk}} \right) \right) / \left( \frac{\partial R_{i-.5jk}^{\theta mom}}{\partial v_{i-.5jk}^{\theta}} \right)$$

# Calculation of dR/dP

$$\begin{aligned} \left( \frac{\partial R_{ijk}^{cont}}{\partial P_{ijk}} \right) &\approx \left( \frac{\partial R_{ijk}^{cont}}{\partial v_{i+.5jk}^\theta} \right) \left( \frac{\partial R_{i+.5jk}^{\theta mom}}{\partial P_{ijk}} \right) / \left( \frac{\partial R_{i+.5jk}^{\theta mom}}{\partial v_{i+.5jk}^\theta} \right) + \left( \frac{\partial R_{ijk}^{cont}}{\partial v_{i-.5jk}^\theta} \right) \left( \frac{\partial R_{i-.5jk}^{\theta mom}}{\partial P_{ijk}} \right) / \left( \frac{\partial R_{i-.5jk}^{\theta mom}}{\partial v_{i-.5jk}^\theta} \right) \\ &+ \left( \frac{\partial R_{ijk}^{cont}}{\partial v_{ij+.5k}^\phi} \right) \left( \frac{\partial R_{ij+.5k}^{\phi mom}}{\partial P_{ijk}} \right) / \left( \frac{\partial R_{ij+.5k}^{\phi mom}}{\partial v_{ij+.5k}^\phi} \right) + \left( \frac{\partial R_{ijk}^{cont}}{\partial v_{ij-.5k}^\phi} \right) \left( \frac{\partial R_{ij-.5k}^{\phi mom}}{\partial P_{ijk}} \right) / \left( \frac{\partial R_{ij-.5k}^{\phi mom}}{\partial v_{ij-.5k}^\phi} \right) \\ &+ \left( \frac{\partial R_{ijk}^{cont}}{\partial v_{ijk+.5}^r} \right) \left( \frac{\partial R_{ijk+.5}^{r mom}}{\partial P_{ijk}} \right) / \left( \frac{\partial R_{ijk+.5}^{r mom}}{\partial v_{ijk+.5}^r} \right) + \left( \frac{\partial R_{ijk}^{cont}}{\partial v_{ijk-.5}^r} \right) \left( \frac{\partial R_{ijk-.5}^{r mom}}{\partial P_{ijk}} \right) / \left( \frac{\partial R_{ijk-.5}^{r mom}}{\partial v_{ijk-.5}^r} \right) \end{aligned}$$



A quick examination of  $(\partial R^{cont} / \partial P)$  reveals that it scales as  $1/\text{viscosity}$ , as follows. If  $h$  represents grid spacing, then  $(\partial R^{cont} / \partial v) \approx 1/h$ ,  $(\partial R^{mom} / \partial P) \approx 1/h$ , and  $(\partial R^{mom} / \partial v) \approx \eta/h^2$ . Thus, the pressure correction in a cell can be approximated as  $-\eta \nabla \cdot (\rho \underline{v})$ , which was what was used in the original cartesian version of this code (e.g., (Tackley, 1996))

‘pseudo-compressibility’ also gives  $1/\text{viscosity}$  factor (Kameyama)

# Multigrid solvers

- ⊙ Gauss-Seidel or Jacobi iterations effectively smooth short-wavelength error (residual) but long-wavelengths take a long time
- ⊙ Therefore smooth the residual on grids with 2\* the spacing, then 4\* spacing, 8\* spacing etc.
- ⊙ Ideally leads to convergence in fixed #iter regardless of grid size
- ⊙ Problem: if viscosity varies rapidly, not correctly represented at coarse levels => slow or non-convergence

# Multigrid cycles

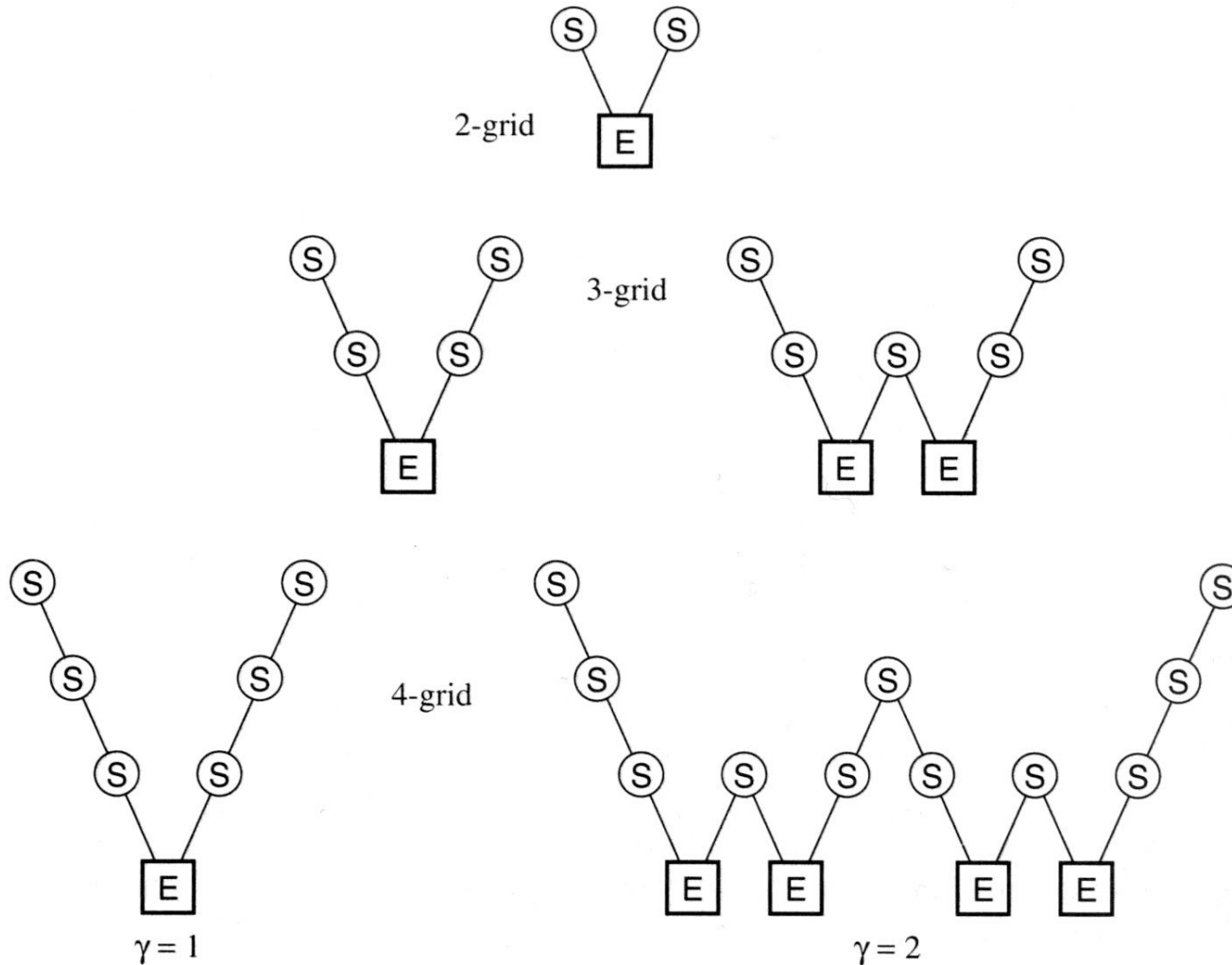
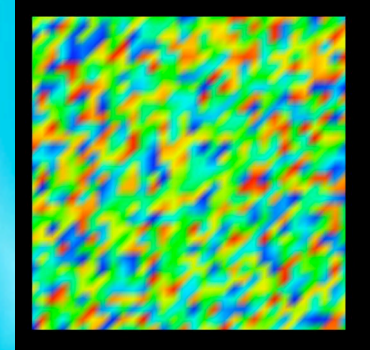


Figure 19.6.1. Structure of multigrid cycles. S denotes smoothing, while E denotes exact solution on the coarsest grid. Each descending line \ denotes restriction ( $\mathcal{R}$ ) and each ascending line / denotes prolongation ( $\mathcal{P}$ ). The finest grid is at the top level of each diagram. For the V-cycles ( $\gamma = 1$ ) the E step is replaced by one 2-grid iteration each time the number of grid levels is increased by one. For the W-cycles ( $\gamma = 2$ ), each E step gets replaced by two 2-grid iterations.

# Example: Scalar Poisson eqn.

$$\nabla^2 u = f$$



Finite-difference approximation:

$$\frac{1}{(\Delta x)^2} \left( u_{i,j+1} + u_{i,j-1} + u_{i+1,j} + u_{i-1,j} - 4u_{i,j} \right) = f_{ij}$$

Use iterative approach=>start with  $u=0$ , sweep through grid updating  $u$  values according to:

$$\tilde{u}_{ij}^{n+1} = \tilde{u}_{ij}^n + \alpha R_{ij} \frac{(\Delta x)^2}{4}$$

Where  $R_{ij}$  is the **residue** (“error”):  $R = \nabla^2 \tilde{u} - f$



# Residue after repeated iterations

Start

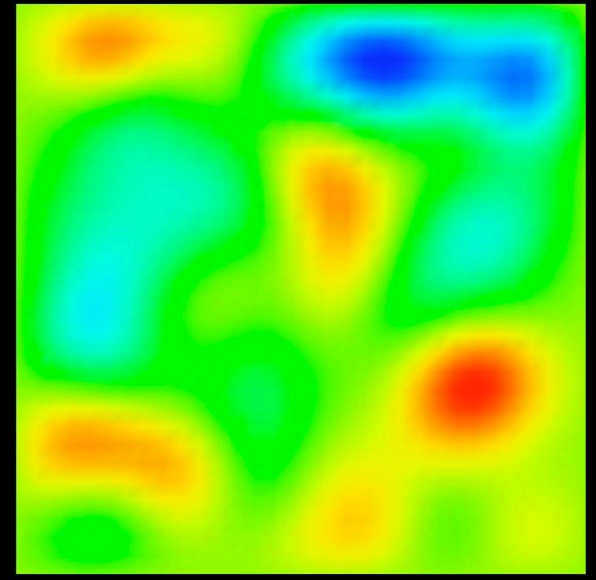
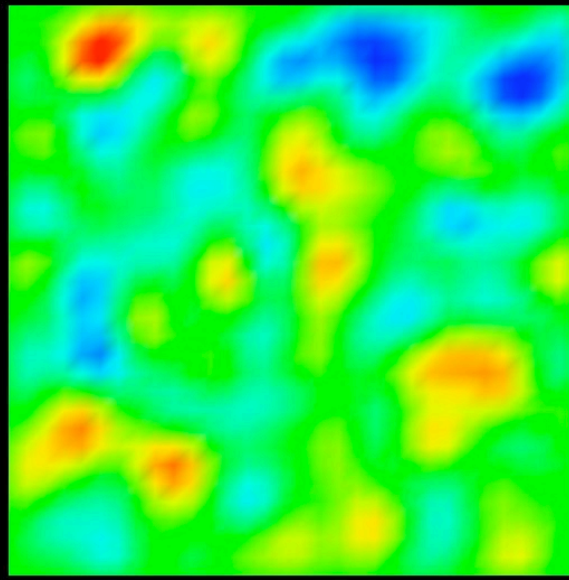
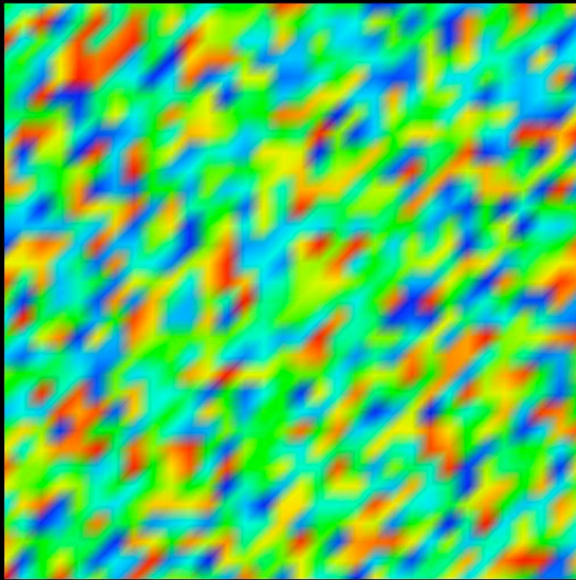
rms residue=0.5

5 iterations

Rms residue=0.06

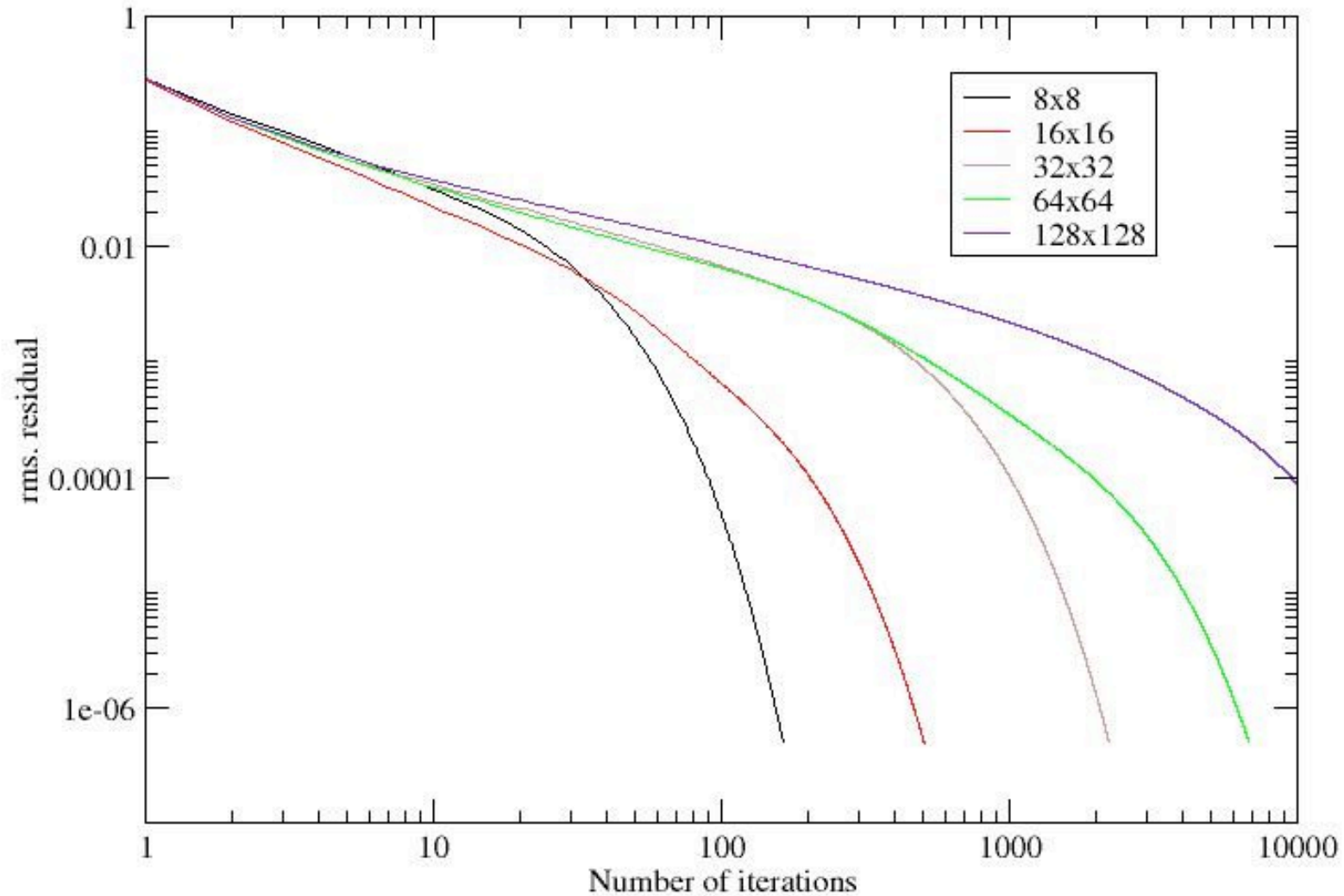
20 iterations

Rms residue=0.025



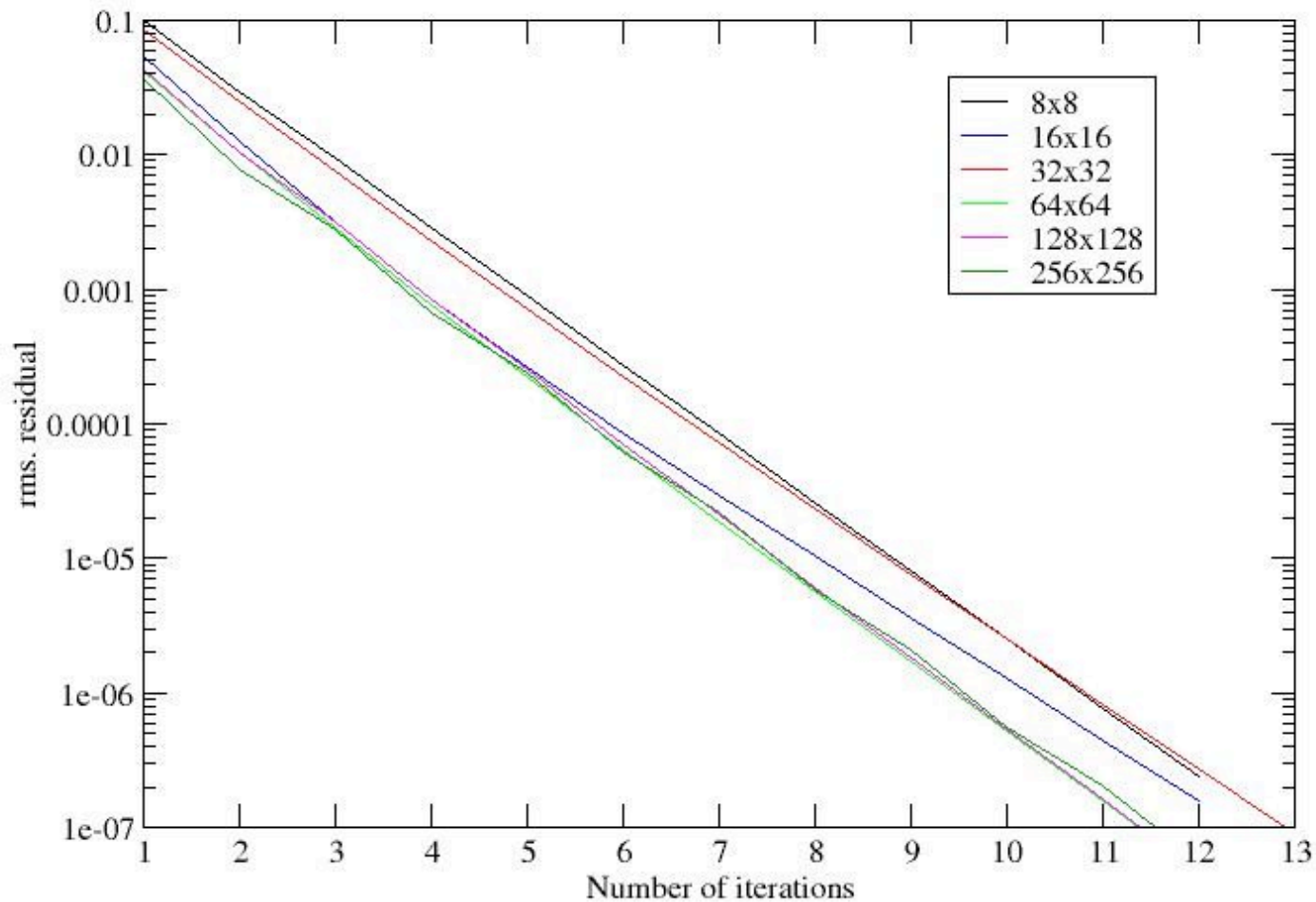
Residue gets smoother => iterations are like a diffusion process

## Scalar Poisson problem - fine grid iters



© Convergence rate decreases as  $N$  increases

## Scalar Poisson problem - MULTIGRID



⊙ Convergence rate **independent of grid size**

⊙  $\Rightarrow$  #operations scales as #grid points

# Multigrid viscous flow solvers are well established in the community

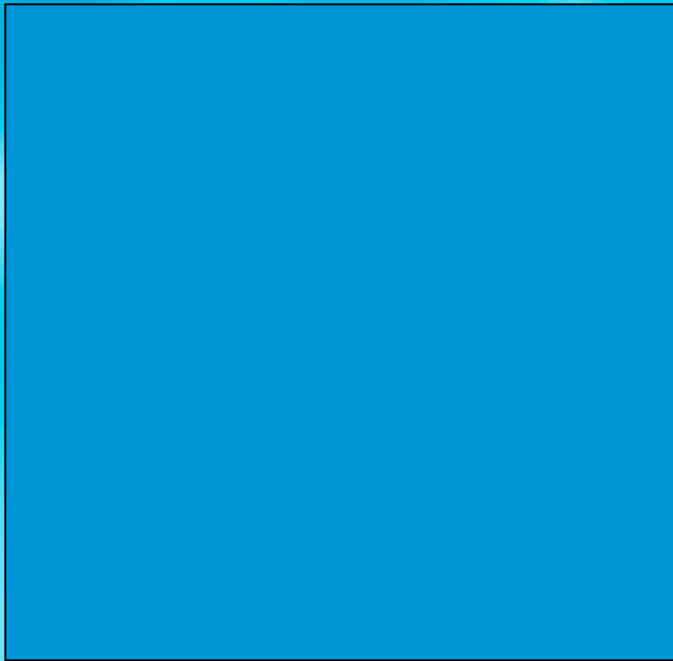
- ⊙ Finite-difference const visc (potentials)
  - Sotin & Parmentier 1994: Cartesian
- ⊙ Finite volume/difference, primitive variable, variable viscosity
  - Tackley 1993 (compressible)
  - Trompert&Hansen 1996: implicit T, improved viscosity restriction
  - Auth+Harder 1999: 2D, FAS, SCGS smoother
  - Albers 2000: FAS, mesh refinement
  - Hernlund+Tackley 2003: Cubed sphere (constant viscosity)
  - Kameyama 2004: Cartesian, Earth Simulator
  - Choblet 2004: Cubed sphere
  - Tackley 2006: Yin-yang sphere
- ⊙ Finite-element, variable viscosity
  - TERRA (1980s-): Spherical, isocahedral
  - CITCOM (~1993): Cartesian, rectangular
  - CITCOM-S (1997?): Spherical, 8-sided elements

# Parallelization

- ◎ Cartesian or single spherical block
  - Straightforward 3D domain decomposition, simple communication patterns, 100s CPUs
  - Care needed on coarse grids
- ◎ Yin-Yang sphere
  - 2 blocks on different node(s)
  - Each block divided in 4 while maintaining simple communication
  - Then decompose in radius
  - Current version up to 64 cpus.

# Domain decomposition

Single CPU

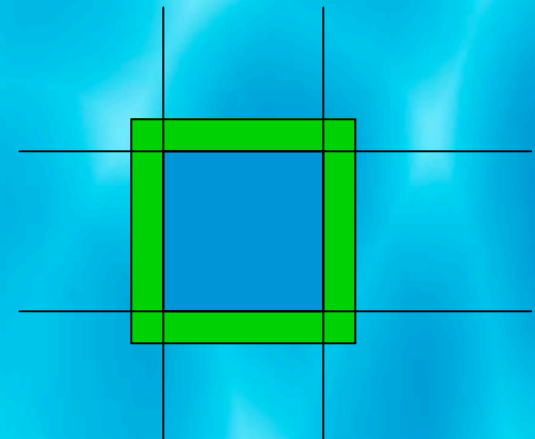
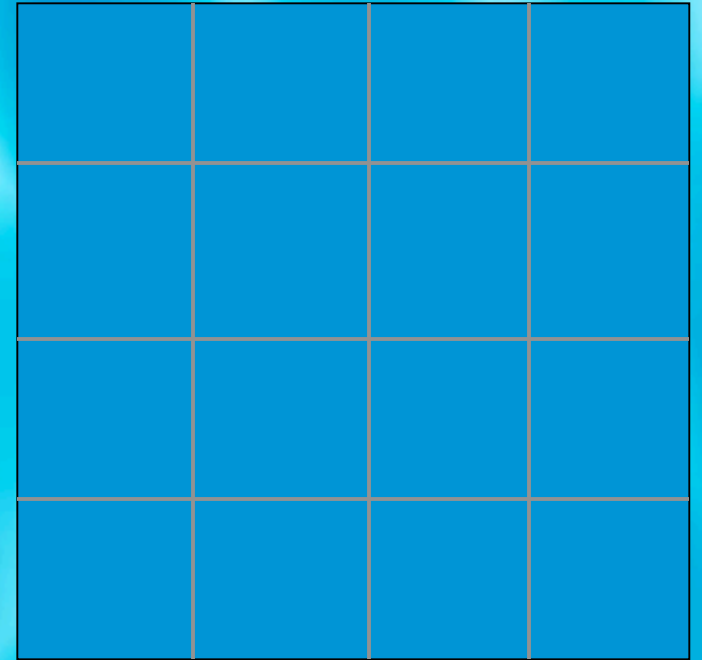


8 CPUs

|       |       |
|-------|-------|
| CPU 0 | CPU 1 |
| CPU 2 | CPU 3 |
| CPU 4 | CPU 5 |
| CPU 6 | CPU 7 |

# Boundaries

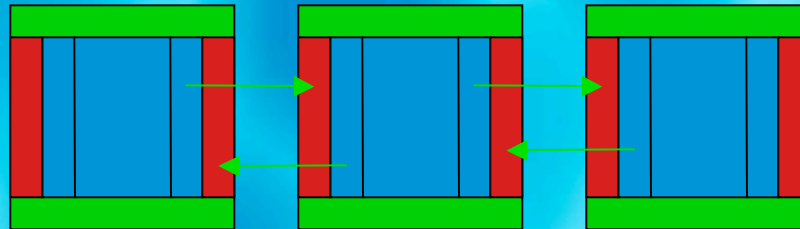
- ⦿ When updating points at edge of subdomain, need values on neighboring subdomains
- ⦿ Hold copies of these locally using “ghost points”
- ⦿ This minimizes # of messages, because they can be updated all at once instead of individually



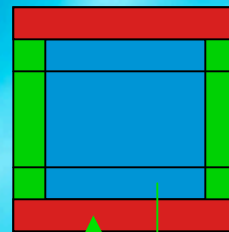
■ =ghost points

# Boundary communication

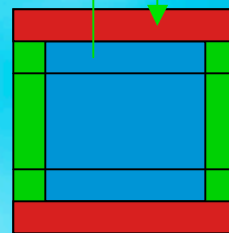
Step 1: x-faces



Step 2: y-faces (including corner values from step 1)



[Step 3: z-faces (including corner values from steps 1 & 2)]

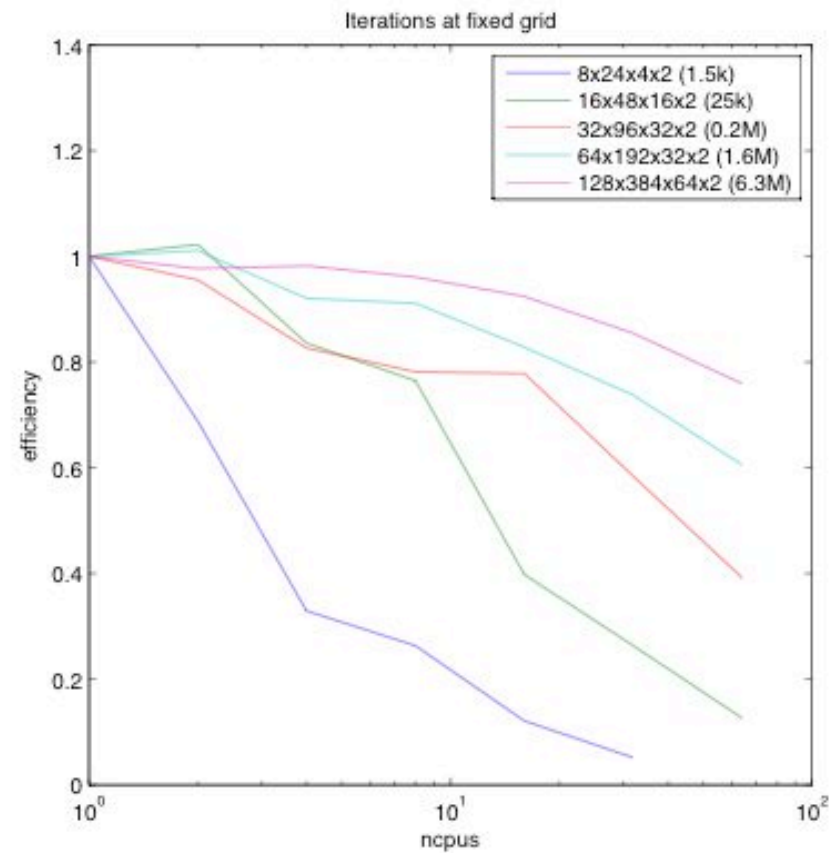
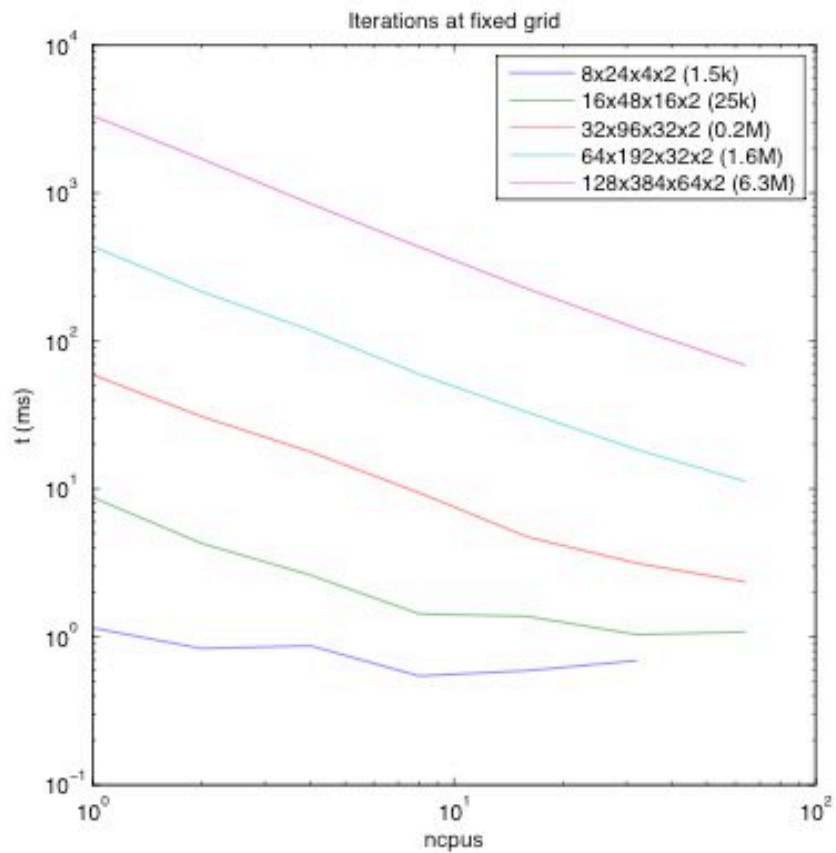
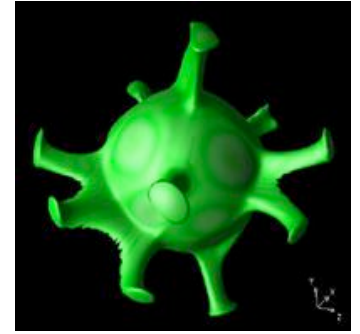


Doing the 3 directions sequentially avoids the need for additional messages to do edges & corners (=>in 3D, 6 messages instead of 26)

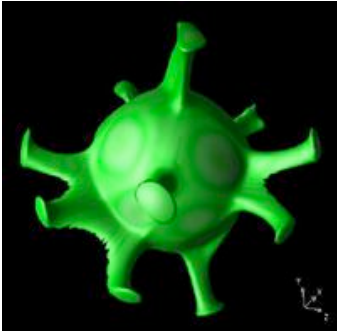


# StagYY Performance

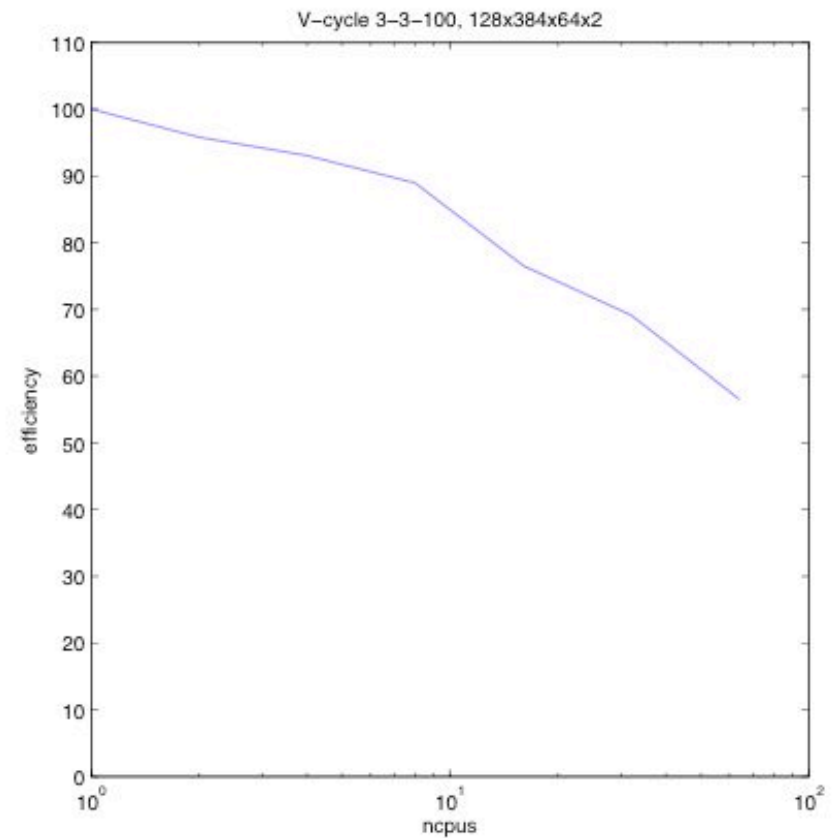
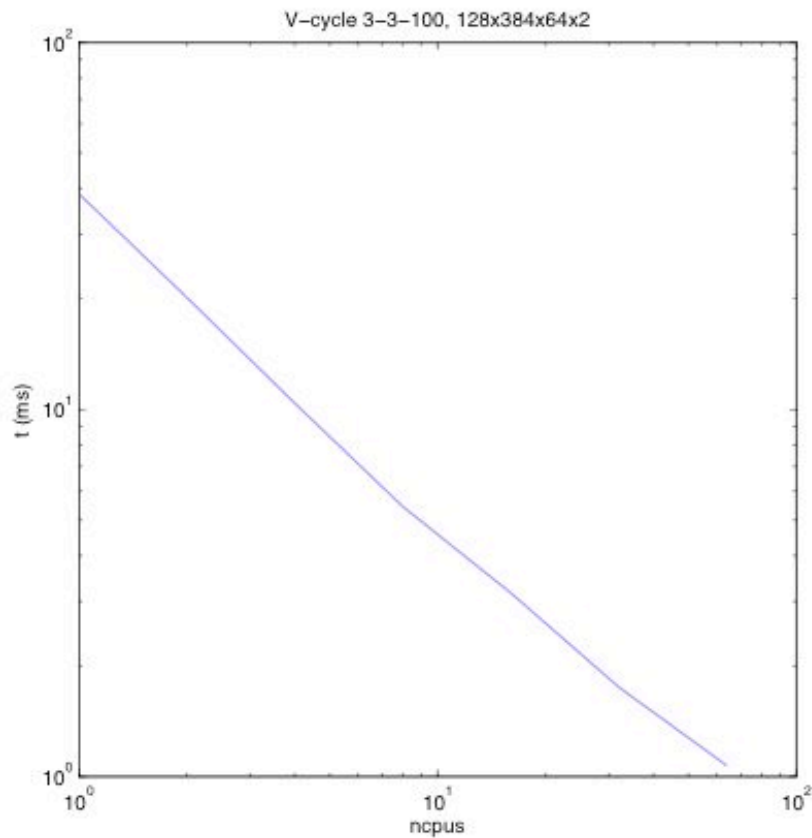
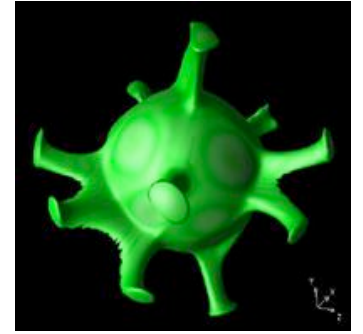
# YY iterations on Gonzales (dual-Opteron cluster, Quadrics interconnect)



⊙ Efficiency OK with ~millions of cells

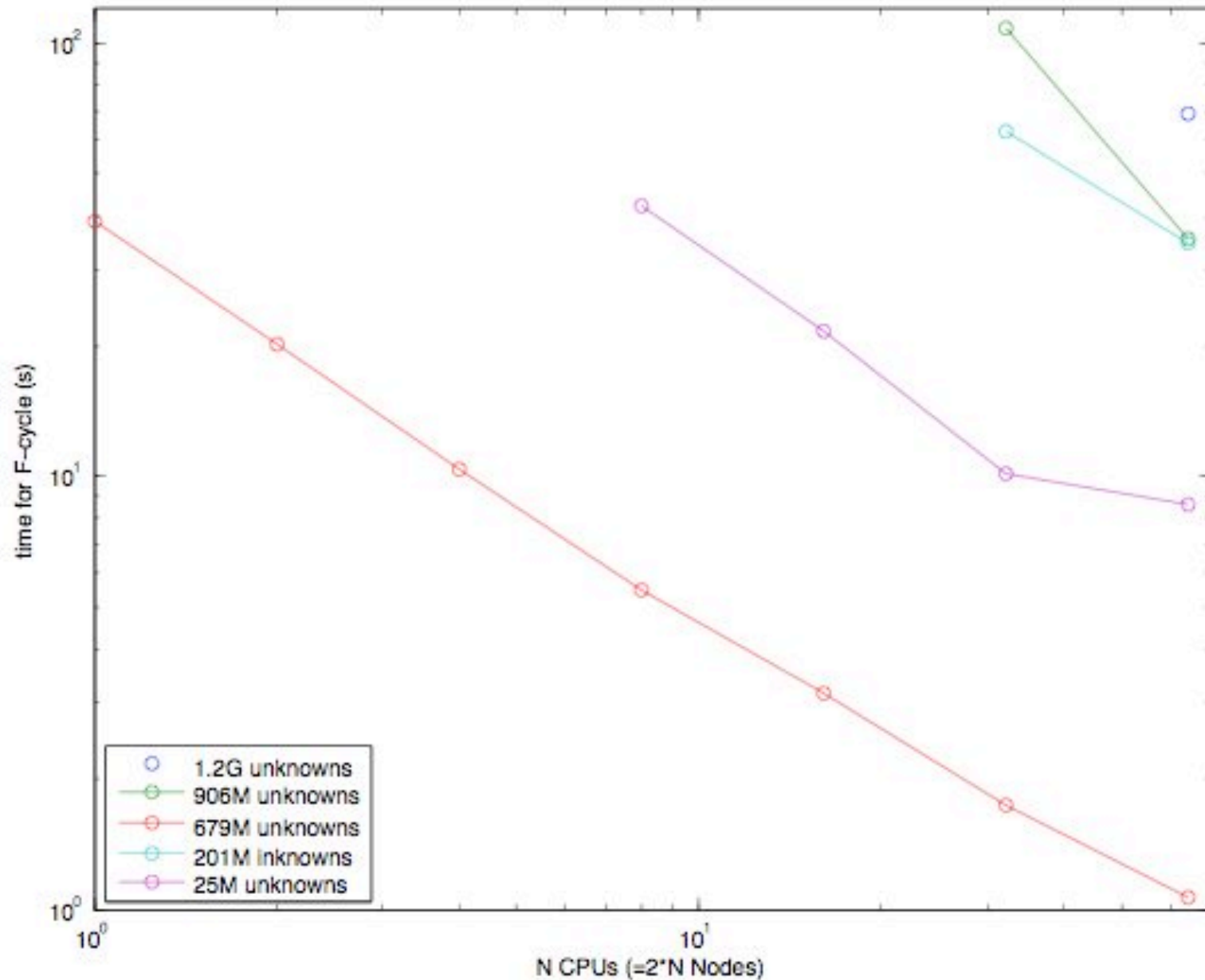


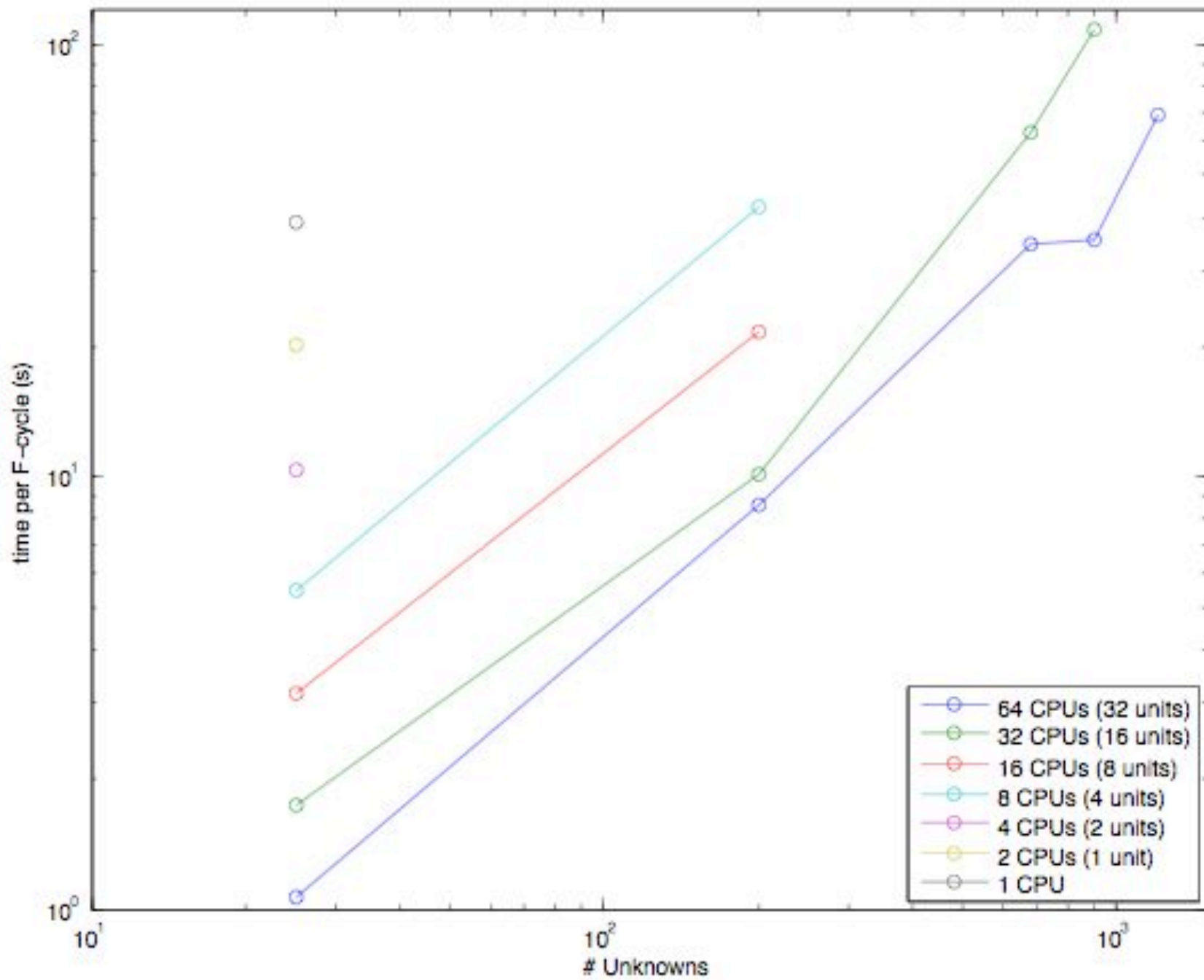
# YY multigrid V-cycles (6.3 M cells)

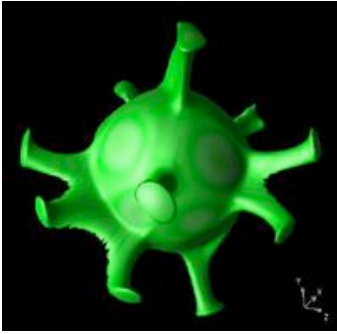


- ⊙ Could be better
- ⊙ Will be better (more points, cell relax)

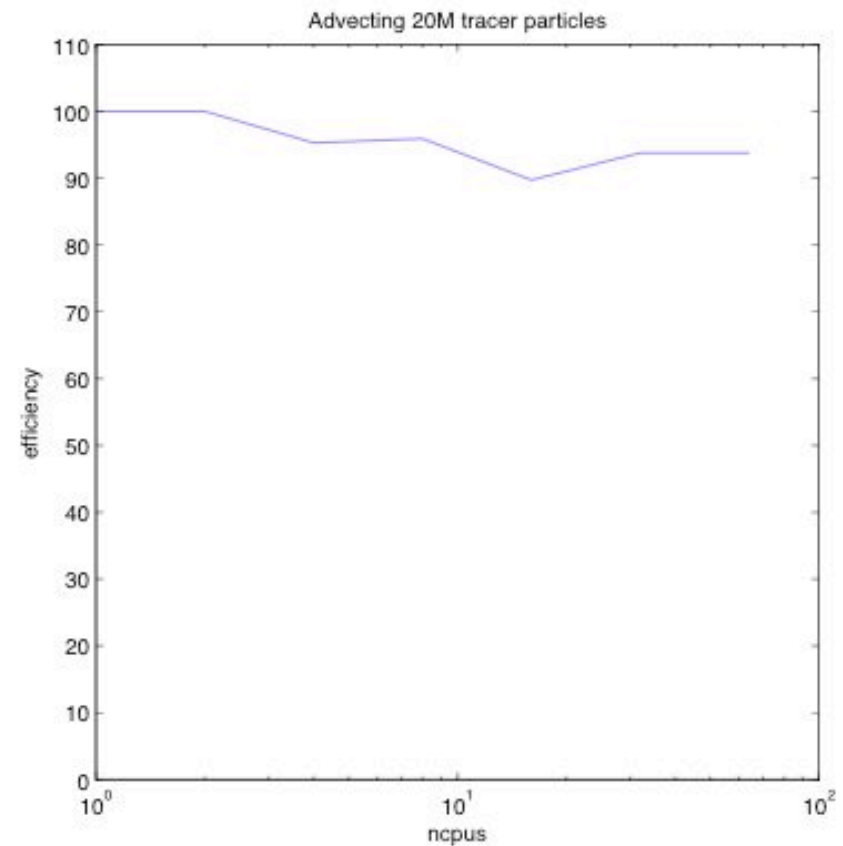
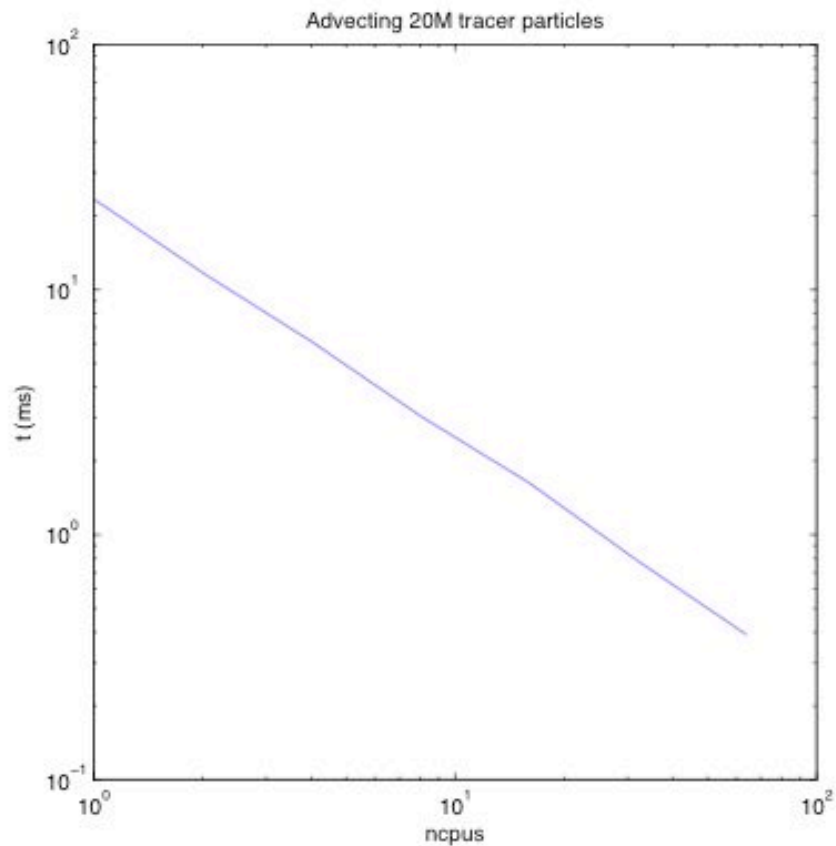
Up to 1.2 billion unknowns on only 32 nodes (64 cpus)







# Advecting 20M tracers

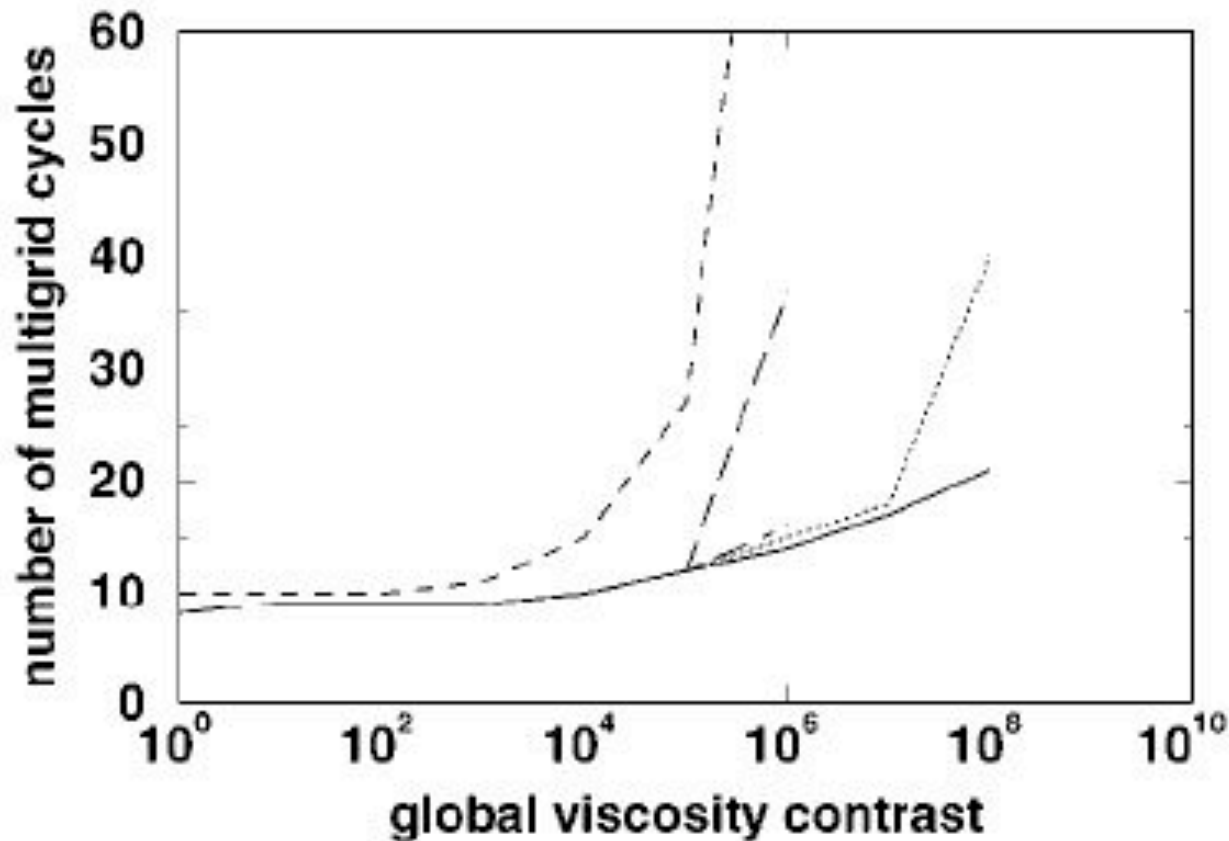


⦿ Excellent efficiency

# How about other aspects of performance?

- ⦿ The main problem facing these codes is lack of robustness to large viscosity variations (e.g., orders of magnitude per grid point)
- ⦿ Accurate treatment of non-diffusive chemical variations is also a major challenge

# Problem: Not robust with large viscosity variations!



From Albers 2000

V=dashed

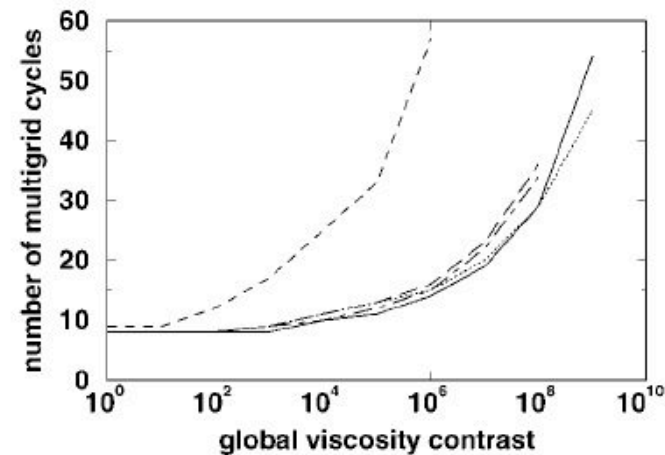
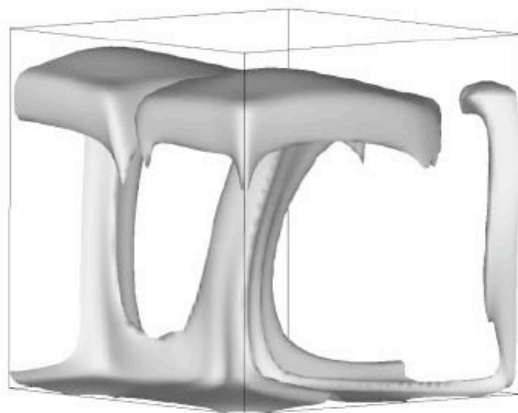
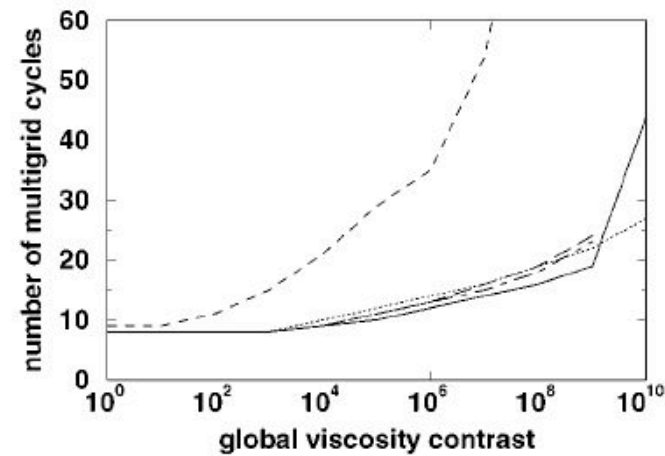
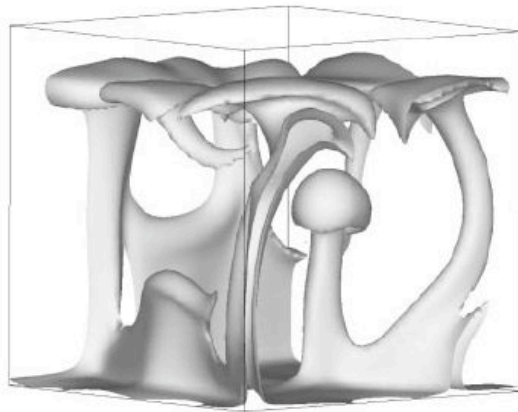
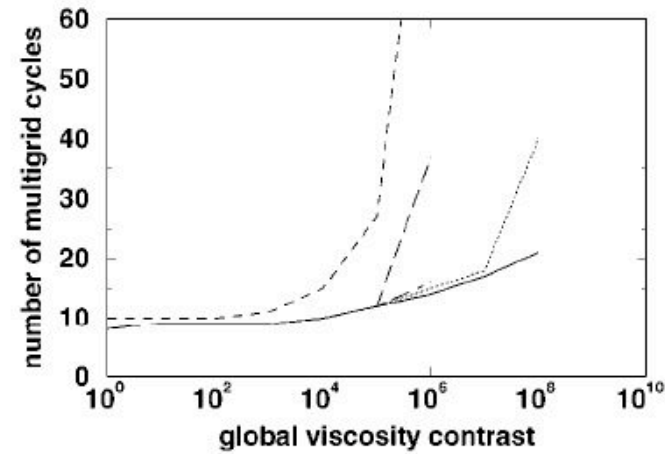
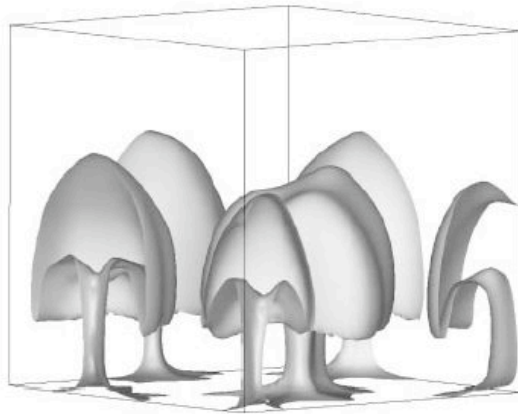
F=long-dashed

W=dot-dashed

Mod-V (dotted)

Mod-W (solid)





From Albers  
 V=dashed  
 F=long-dashed  
 W=dot-dashed  
 Mod-V (dotted)  
 Mod-W (solid)

- ⊙ Convergence depends on 3D structure
- ⊙ Additional coarse iterations greatly helps!

# The solution: Matrix-dependent pressure prolongation

The pressure correction is ~proportional to viscosity  
If fine-grid cell has much lower viscosity than coarse-grid cell, correction is much too large => divergence!

Tried weighting prolongation according to viscosity:  
can help, but sometimes gets worse

Instead weight using  $\left(\frac{dR}{dP}\right)_{ijk} = \frac{d(\nabla \cdot \vec{v})_{ijk}}{dP_{ijk}}$

# Prolongation & restriction on staggered grid

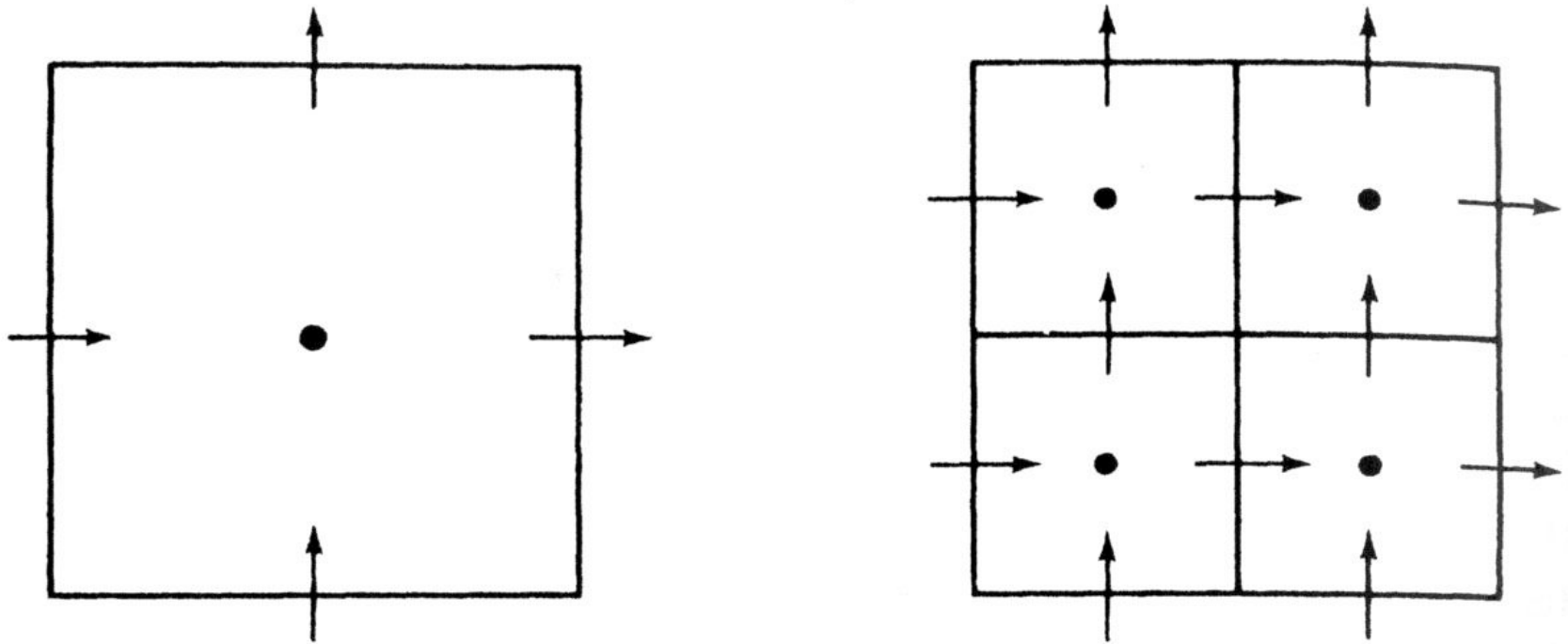


*Figure 9.7.3* Coarse and fine grid cells.

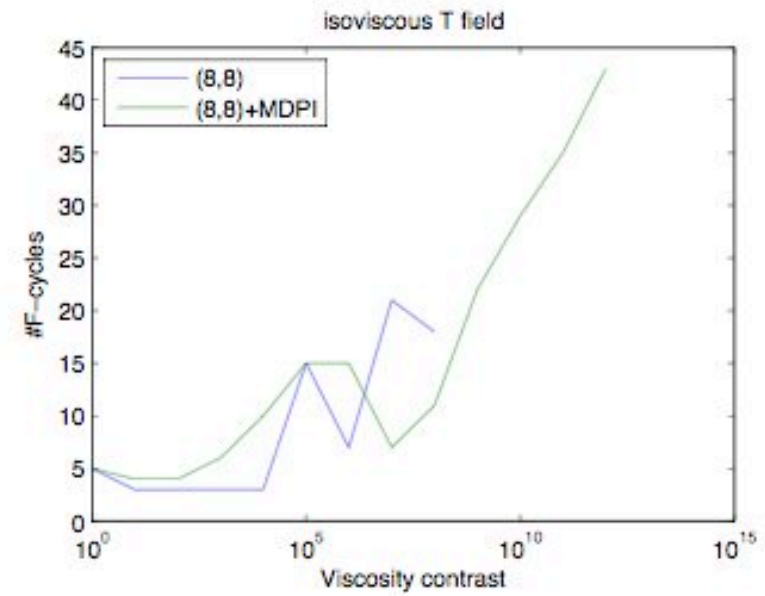
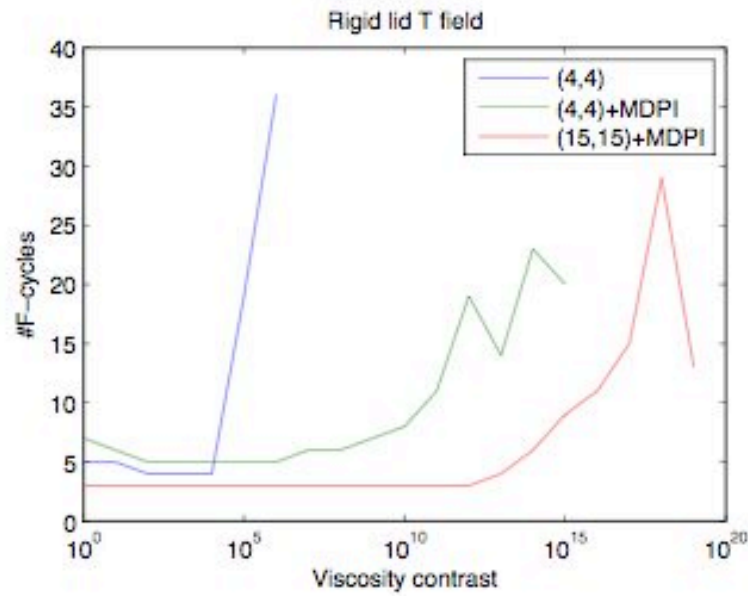
# Matrix-dependent pressure prolongation scheme

$$\delta P_{fine} = C \delta P_{coarse} / \left( \frac{dR_{cont}}{dP} \right)_{fine}$$

$$\frac{1}{8} \sum \delta P_{fine} = \delta P_{coarse}$$

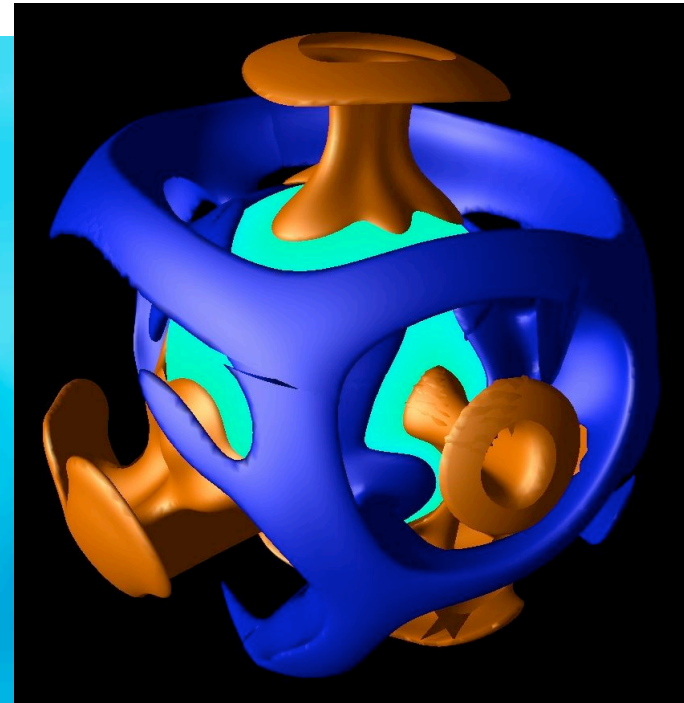
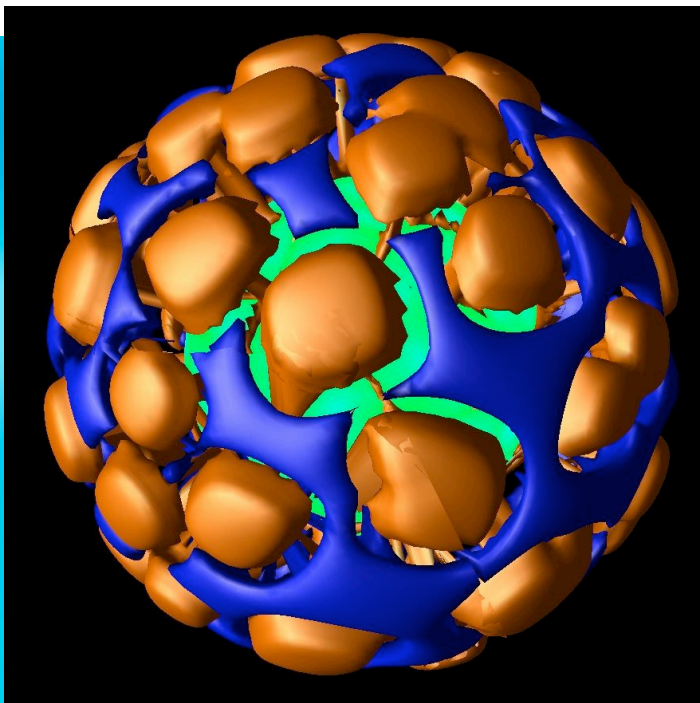
$$C = 8 \left( \sum 1 / \left( \frac{dR_{cont}}{dP} \right)_{fine} \right)^{-1}$$

Robust for any viscosity field (so far)

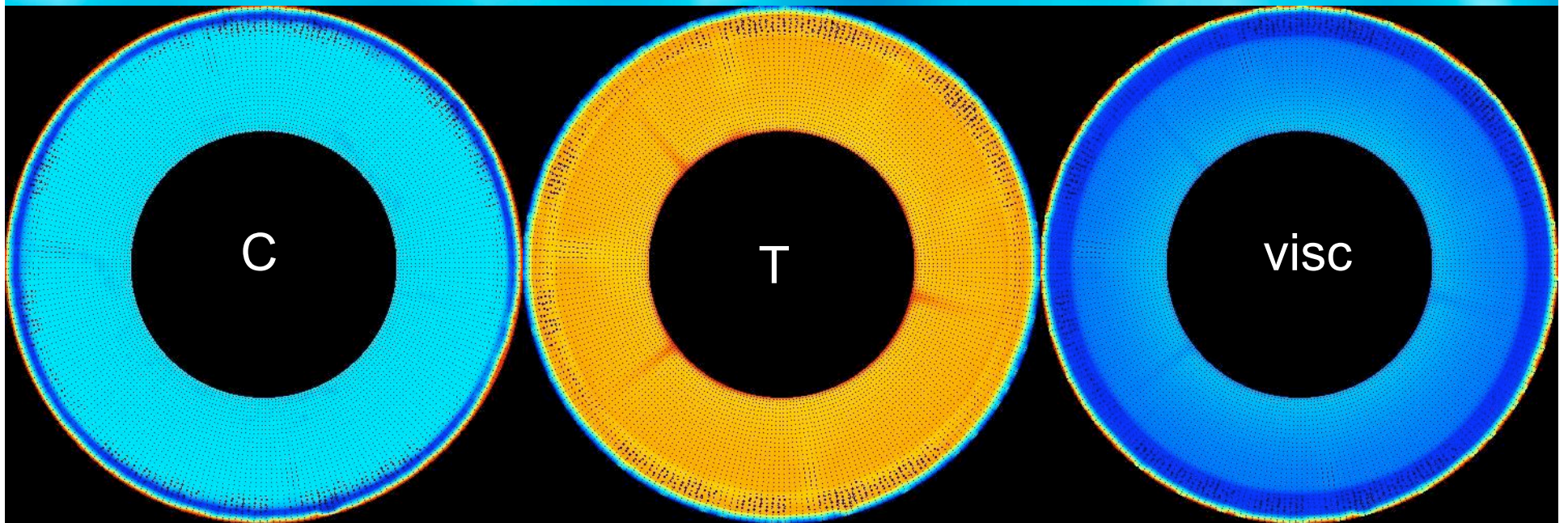


54000\* between adjacent points

196000\* between adjacent points



# ROBUST to large viscosity variations

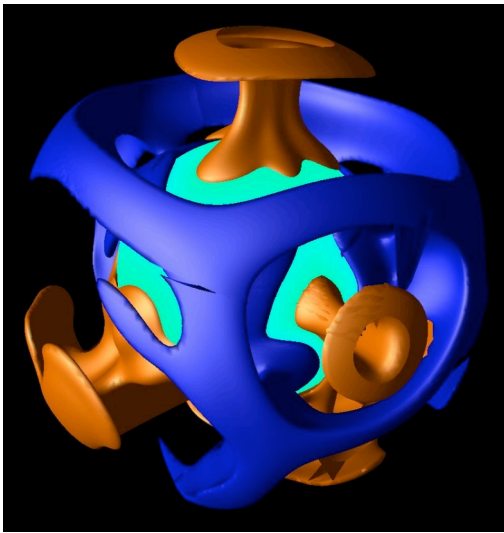


⦿ Case above has 13+ orders of magnitude total, 6 orders between adjacent cells

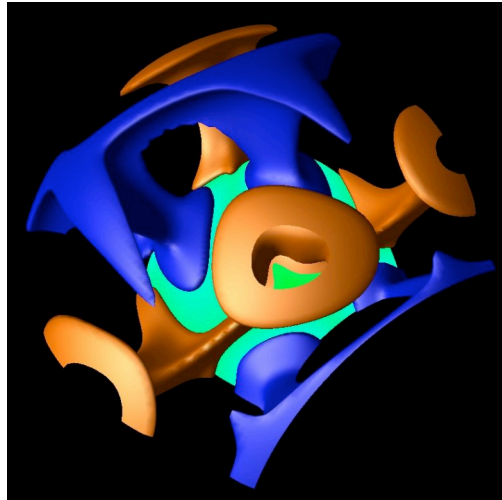
# Geometries modelled

Change with single switch

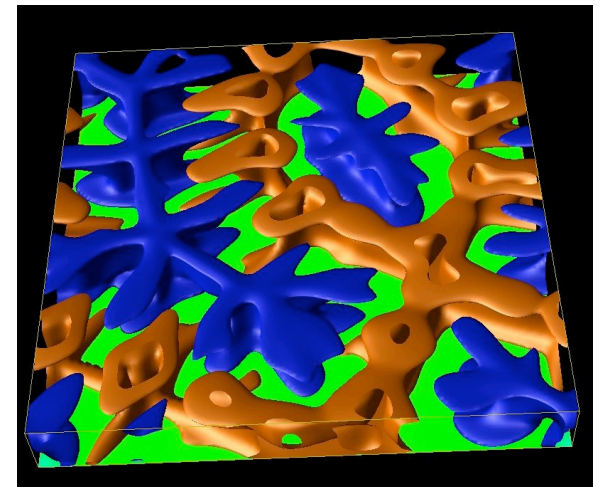
full sphere



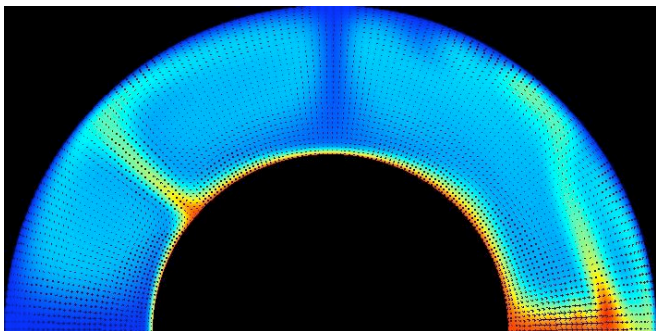
regional spherical



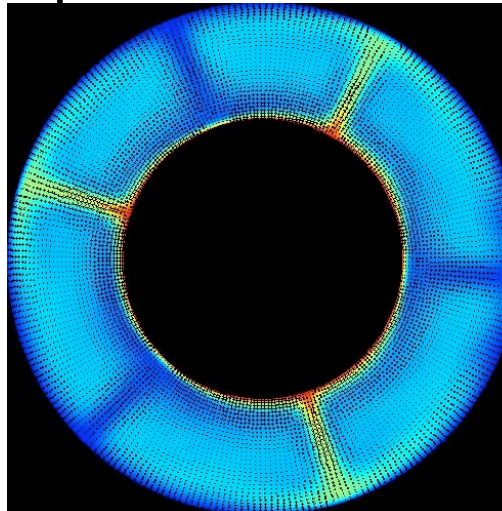
Cartesian -3D



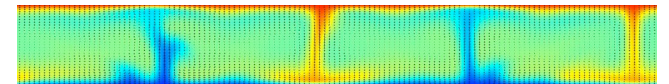
Spherical axisymmetric



Spherical annulus



-2D



# 2D Spherical Annulus geometry (Hernlund & Tackley, 2008)

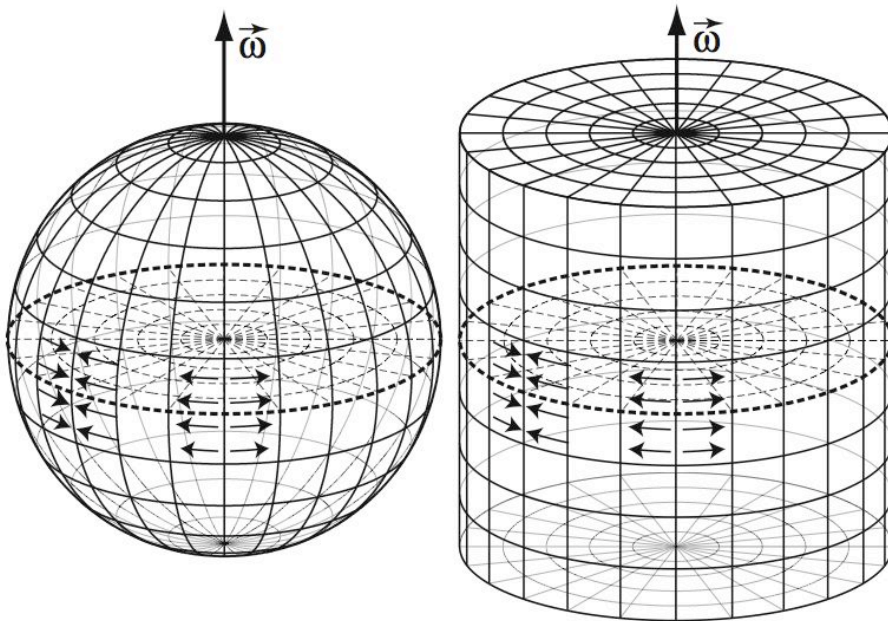


Figure 1: Comparison between the 2D approximations for rigid body translations on the surface of a sphere (left) and a cylinder (right), with the circular 2D slice of interest indicated by dashed lines. Arrows are shown to indicate a divergent motion such as that along a mid-ocean ridge as well as convergent motion such as a subduction zone setting. In both cases, the angular velocity vector  $\vec{\omega}$  describing the 2D lateral motions in the slice is directed along the axes of the coordinate systems if they are taken to be oriented perpendicular to the slice. The primary difference between the two descriptions is that motions on a sphere are projected onto a surface with two degrees of curvature, while a cylinder has only one degree of curvature.

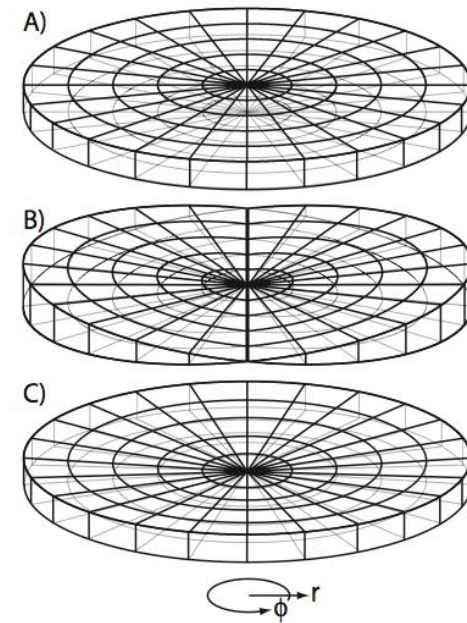


Figure 2: Illustration of what is meant by the “virtual” thickness  $J/r$  of a 2D circular slice through a 3D grid. In the constant thickness case (A), representative of a cylindrical model with effective Jacobian  $J = r$ , the virtual thickness is constant everywhere. For a variable thickness in the angular direction (B), representative of a spherical axi-symmetric grid with effective Jacobian  $J = r^2 \sin \phi$ , the virtual thickness depends on the angular location in the grid and the radius. In the variable radial thickness case (C) with effective Jacobian  $J = r^2$ , the virtual thickness increases with distance from the center of the grid without any angular dependence.



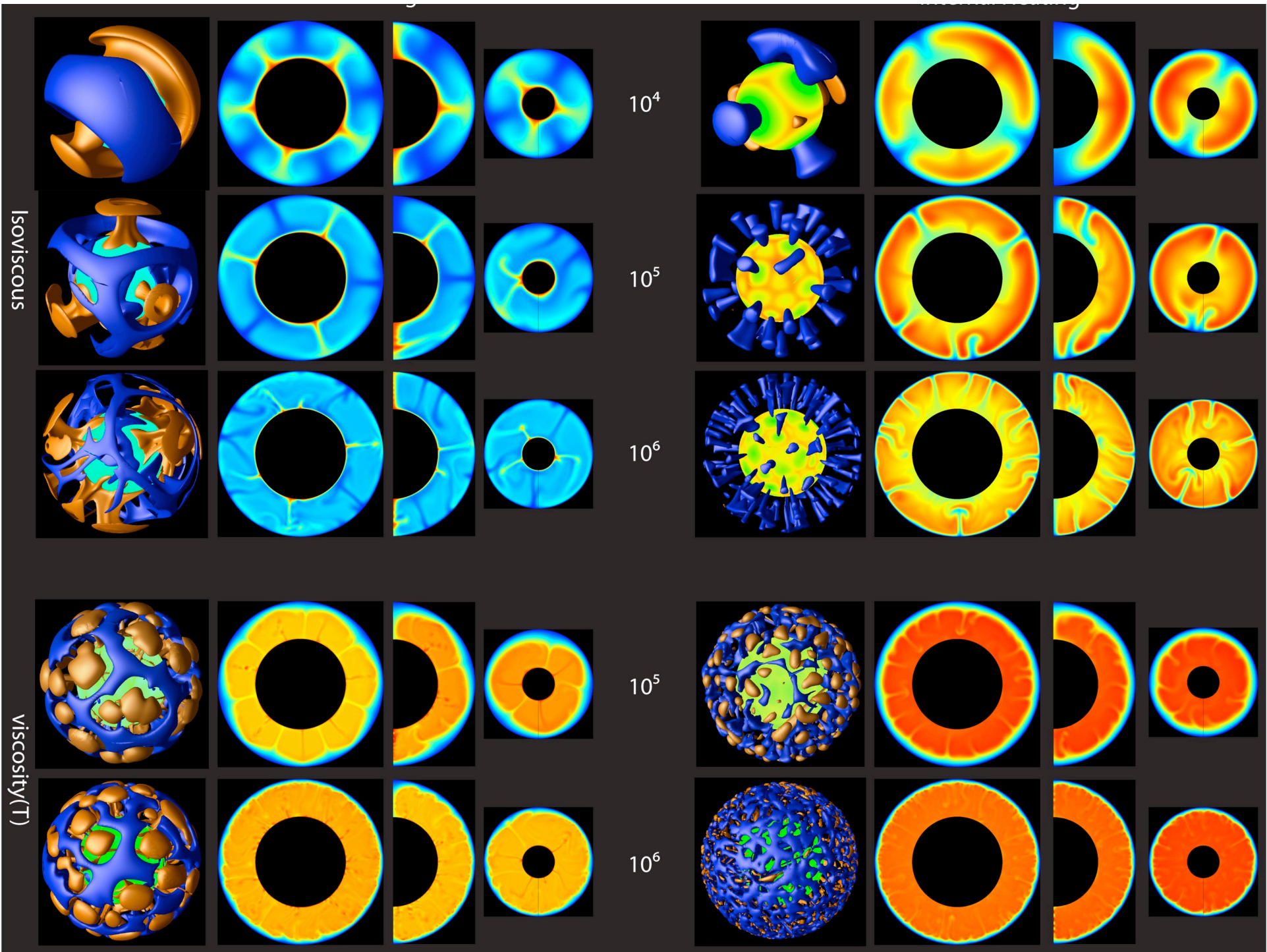


Table 1. Basal heated, isoviscous convection

| Ra     | Geometry     | $\langle \text{Nu} \rangle$ | $\Delta \text{Nu}_{\text{peak-peak}}$ | $\langle V_{\text{rms}} \rangle$ | $\Delta(V_{\text{rms}})_{\text{pk-pk}}$ |
|--------|--------------|-----------------------------|---------------------------------------|----------------------------------|---|
| $10^4$ | 3D           | 3.85                        | steady                                | 42.3                             | 0                                       |
|        | annulus      | 4.18                        | steady                                | 37.7                             | 0                                       |
|        | axisymmetric | 4.01                        | steady                                | 41.0                             | 0                                       |
|        | cylindrical  | 3.99                        | steady                                | 35.6                             | 0                                       |
| $10^5$ | 3D           | 7.27                        | 0.5                                   | 160                              | 11                                      |
|        | annulus      | 7.39                        | 0.3                                   | 160                              | 14                                      |
|        | axisymmetric | 7.26                        | 3.2                                   | 159                              | 100                                     |
|        | cylindrical  | 6.2                         | 2.1                                   | 165                              | 90                                      |
| $10^6$ | 3D           | 15.9                        | 1.3                                   | 625                              | 80                                      |
|        | annulus      | 14.4                        | 3.4                                   | 640                              | 275                                     |
|        | axisymmetric | 13.7                        | 6.0                                   | 520                              | 500                                     |
|        | cylindrical  | 14.4                        | 5.5                                   | 613                              | 460                                     |

Table 2. Basal heated, temperature-dependent viscosity convection

| $\text{Ra}_{1/2}$ | Geometry     | $\langle \text{Nu} \rangle$ | $\Delta \text{Nu}^*_{\text{peak-peak}}$ | $\langle V_{\text{rms}} \rangle$ | $\Delta(V_{\text{rms}})_{\text{pk-pk}}$ |
|-------------------|--------------|-----------------------------|---|----------------------------------|---|
| $10^5$            | 3D           | 6.30                        | 0                                       | 405                              | 5                                       |
|                   | annulus      | 5.71                        | 0.1                                     | 463                              | 90                                      |
|                   | axisymmetric | 5.07                        | 0.2                                     | 450                              | 210                                     |
|                   | cylindrical  | 4.97                        | 0.1                                     | 495                              | 200                                     |
| $10^6$            | 3D           | 9.7                         | 0                                       | 1804                             | 100                                     |
|                   | annulus      | 10.1                        | 0.1                                     | 1390                             | 780                                     |
|                   | axisymmetric | 10.45                       | 0.1                                     | 1370                             | 1040                                    |
|                   | cylindrical  | 10.4                        | 0.1                                     | 1850                             | 1200                                    |

Table 3. Internally heated, isoviscous convection

| Ra     | Geometry     | $\langle T \rangle$ | $\langle V_{\text{rms}} \rangle$ | $\Delta(V_{\text{rms}})_{\text{pk-pk}}$ |
|--------|--------------|---------------------|----------------------------------|---|
| $10^4$ | 3D           | 0.311               | 23.3                             | 0                                       |
|        | annulus      | 0.308               | 23.5                             | 0                                       |
|        | axisymmetric | 0.330               | 25.8                             | 0                                       |
|        | cylindrical  | 0.319               | 22.8                             | 0                                       |
| $10^5$ | 3D           | 0.322               | 60.5                             | 7                                       |
|        | annulus      | 0.349               | 78.5                             | 36                                      |
|        | axisymmetric | 0.357               | 87.0                             | 65                                      |
|        | cylindrical  | 0.384               | 77.0                             | 75                                      |
| $10^6$ | 3D           | 0.337               | 180                              | 10                                      |
|        | annulus      | 0.350               | 265                              | 160                                     |
|        | axisymmetric | 0.349               | 270                              | 225                                     |
|        | cylindrical  | 0.380               | 268                              | 350                                     |

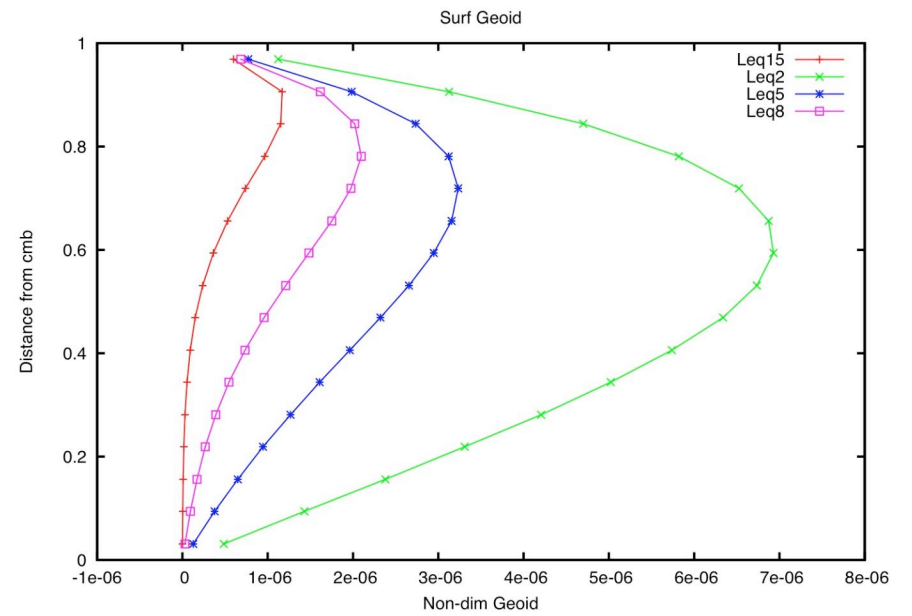
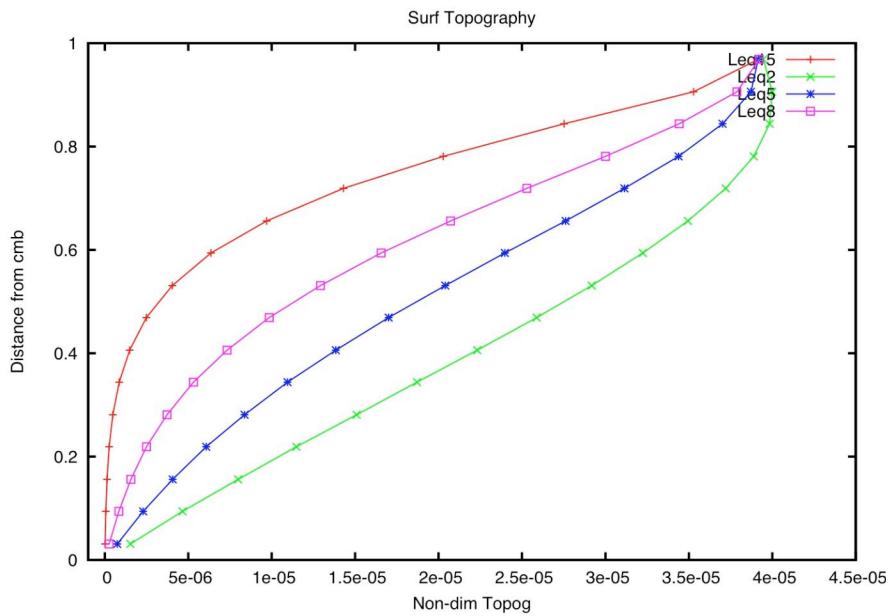
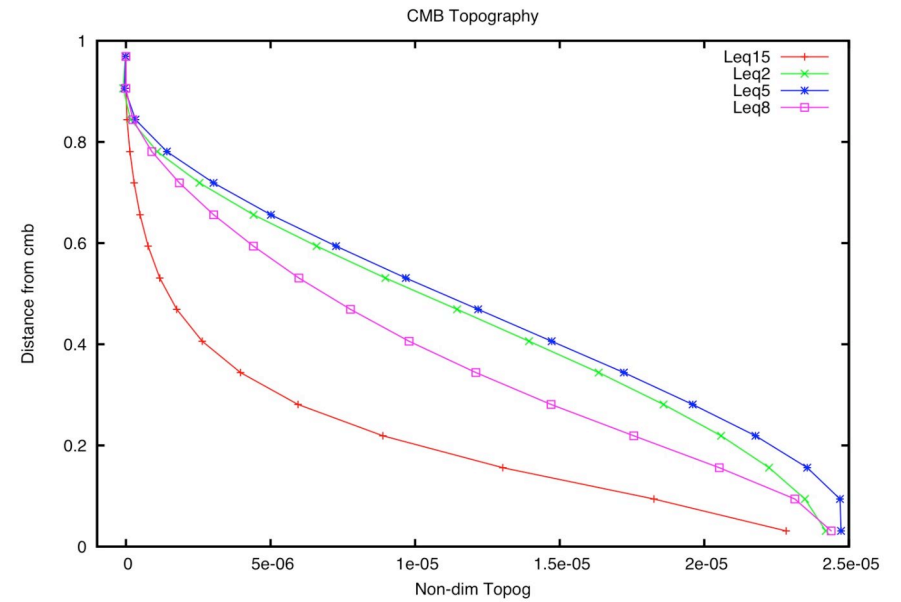
Table 4. Internally heated, temperature-dependent viscosity convection

| $Ra_{1/2}$ | Geometry     | $\langle T \rangle$ | $\langle V_{\text{rms}} \rangle$ | $\Delta(V_{\text{rms}})_{\text{pk-pk}}$ |
|------------|--------------|---------------------|----------------------------------|---|
| $10^5$     | 3D           | 0.587               | 93                               | 4                                       |
|            | annulus      | 0.611               | 135                              | 70                                      |
|            | axisymmetric | 0.610               | 142                              | 95                                      |
|            | cylindrical  | 0.623               | 148                              | 90                                      |
| $10^6$     | 3D           | 0.665               | 565                              | 65                                      |
|            | annulus      | 0.667               | 575                              | 300                                     |
|            | axisymmetric | 0.666               | 560                              | 390                                     |
|            | cylindrical  | 0.690               | 650                              | 430                                     |

# 'Advanced' features

- ◎ Geoid
- ◎ Self-consistent mineralogy

# Geoid & dynamic topography (me, Nakagawa & Stegman)

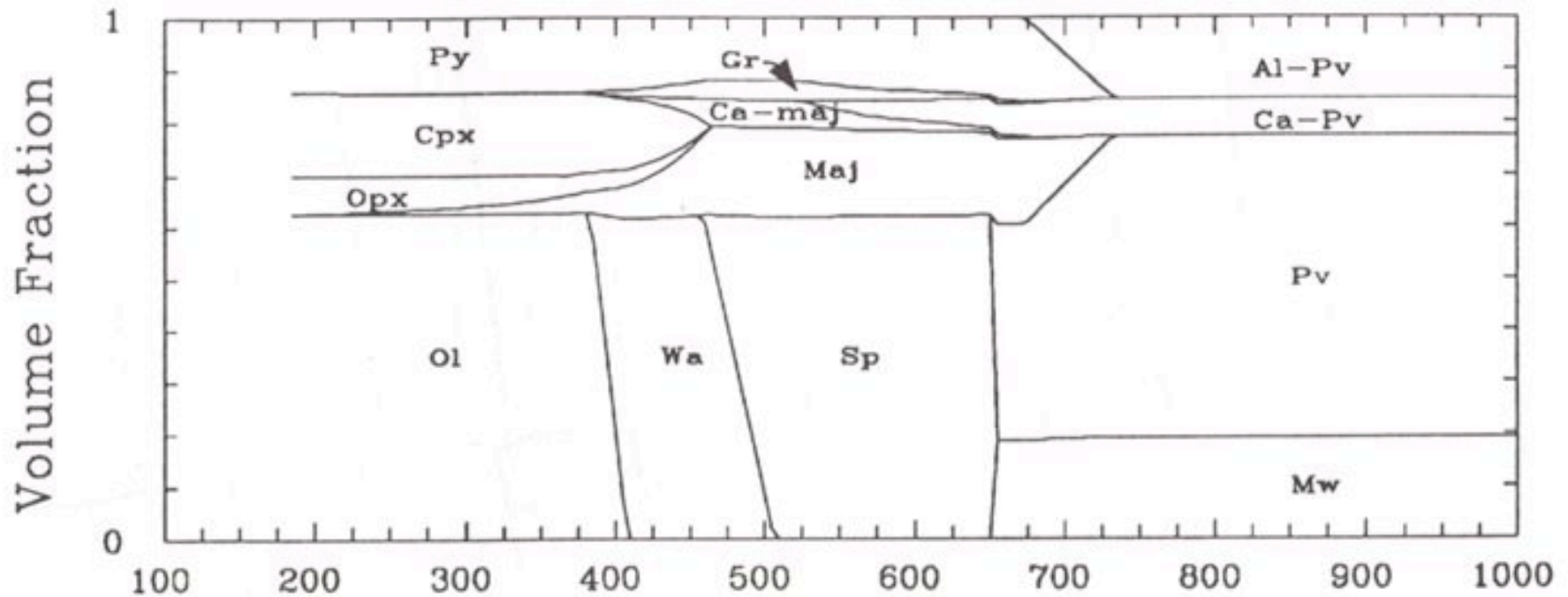


# Self-consistent phase changes / mineralogy (with J. Connolly & F Deschamps)

- ⊙ Mantle rocks have complicated phase diagrams that are only crudely approximated in typical convection calculations
- ⊙ Phase assemblage depends on composition, temperature, pressure
- ⊙ => Calculate phase assemblage and resulting physical properties by minimization of free energy using PERPLEX by J. Connolly
- ⊙ Integrate into large-scale dynamical simulations of thermo-chemical convection of planets

# Mineralogy: complex sequence of composition-dependent phase changes

COMPOSITION A MINERAL PROPORTIONS



© From Ita and Stixrude

# Calculated phase relationships

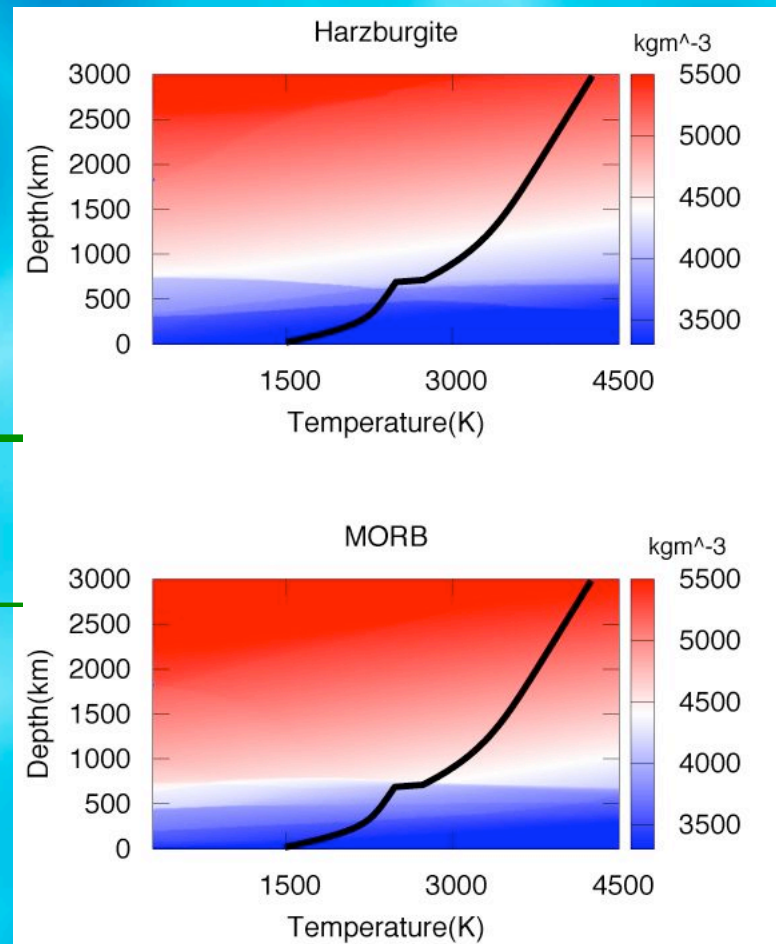
Determined by Free Energy minimization technique: PERPLEX  
[Connolly, 2005]

$$G(T,P) = \sum_i n_i(T,P) \mu_i(T,P)$$

Data for components for two materials from [Stixrude and Lithgow-Bertelloni, 2005]

| Component                      | Harzburgite<br>(mol%) | MORB<br>(mol%) |
|--------------------------------|-----------------------|----------------|
| SiO <sub>2</sub>               | 36.04                 | 41.75          |
| MgO                            | 57.14                 | 22.42          |
| FeO                            | 5.41                  | 6.00           |
| CaO                            | 0.44                  | 13.59          |
| Al <sub>2</sub> O <sub>3</sub> | 0.96                  | 16.24          |

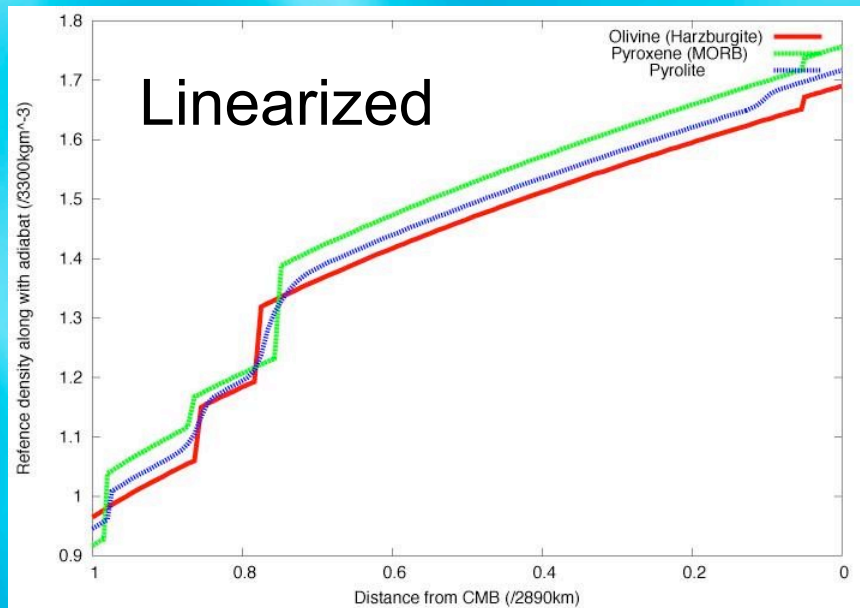
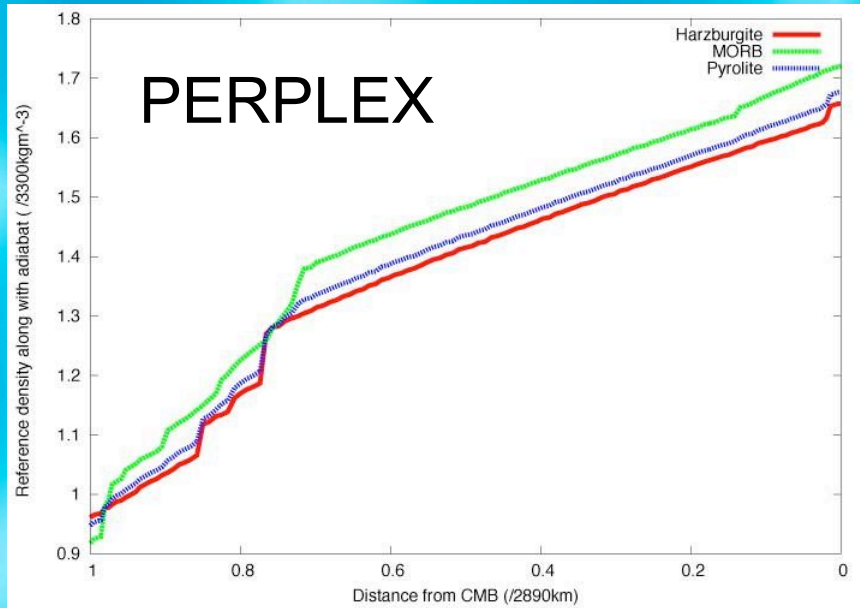
Physical properties (density)



Solid line: Solidus



# Reference density along with adiabat



Pyrolite: Combined two component via amount of MORB composition

- Density difference @ CMB = 2.7% between Harzburgite and MORB (PERPLEX)

= 3.6% (Linearized)

= 2.16% between MORB and Pyrolite (PERPLEX)

= 2.32% (Linearized)

- Olivine-Wadsleyite-Ringwoodite-Perovskite-pPv

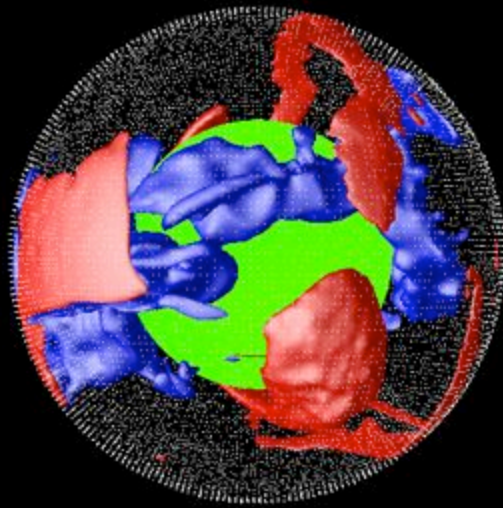
- Px-gt(il or ak)-pv: gradual

- pPv: close to CMB (2800km depth ?)

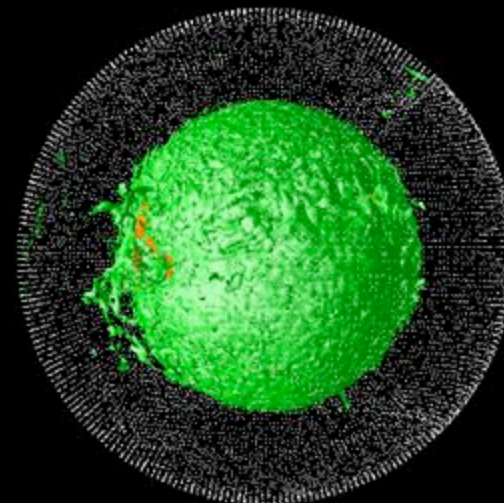
# Numerical example: Thermo-chemical with PERPLEX properties

Time = 4.5 Gyrs after initial state

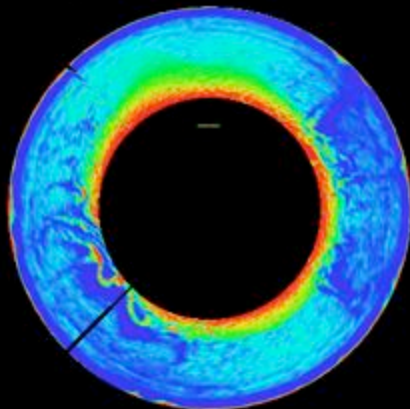
T-residuals (Red: +250K; Blue: -250K)



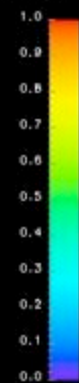
C-isosurface (C=0.75)



Equatorial slice of C

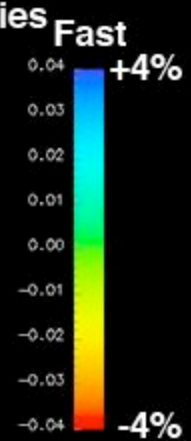
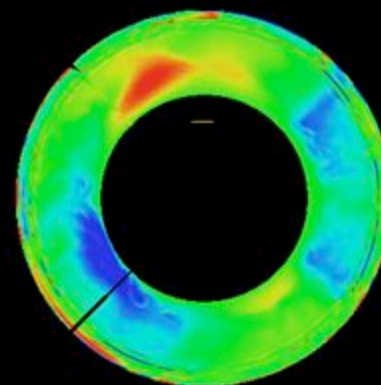


MORB



Harzburgite

Equatorial slice of S-anomalies

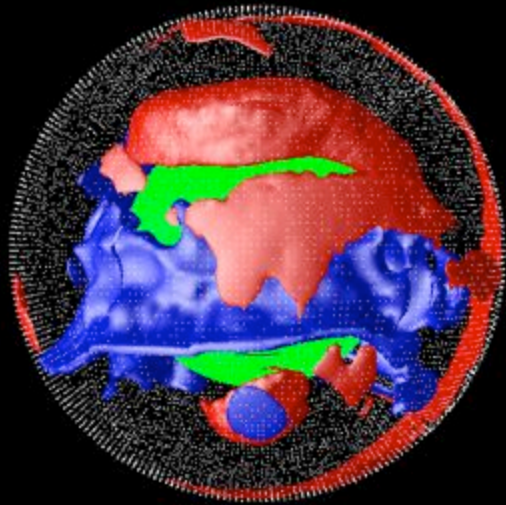


Slow

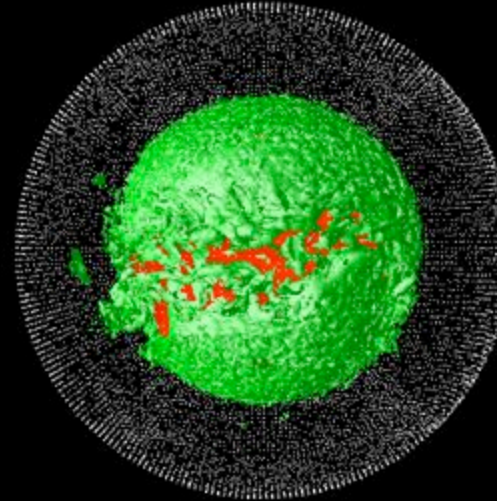
# Numerical example: Linearized properties

Time = 4.5Gyrs after initial state

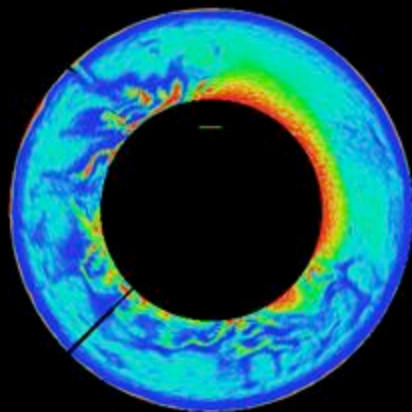
T-residuals (Red: +250K; Blue: -250K)



C-isosurface (C=0.75)



Equatorial slice for C

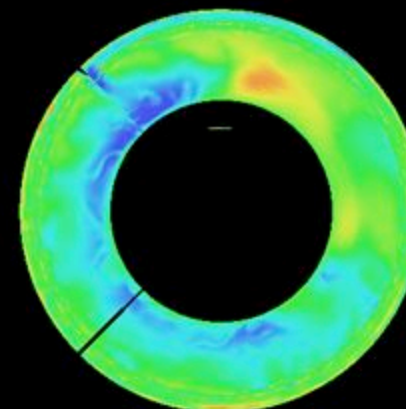


MORB

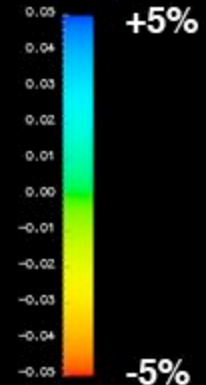


Harzburgite

Equatorial slice for S-anomalies



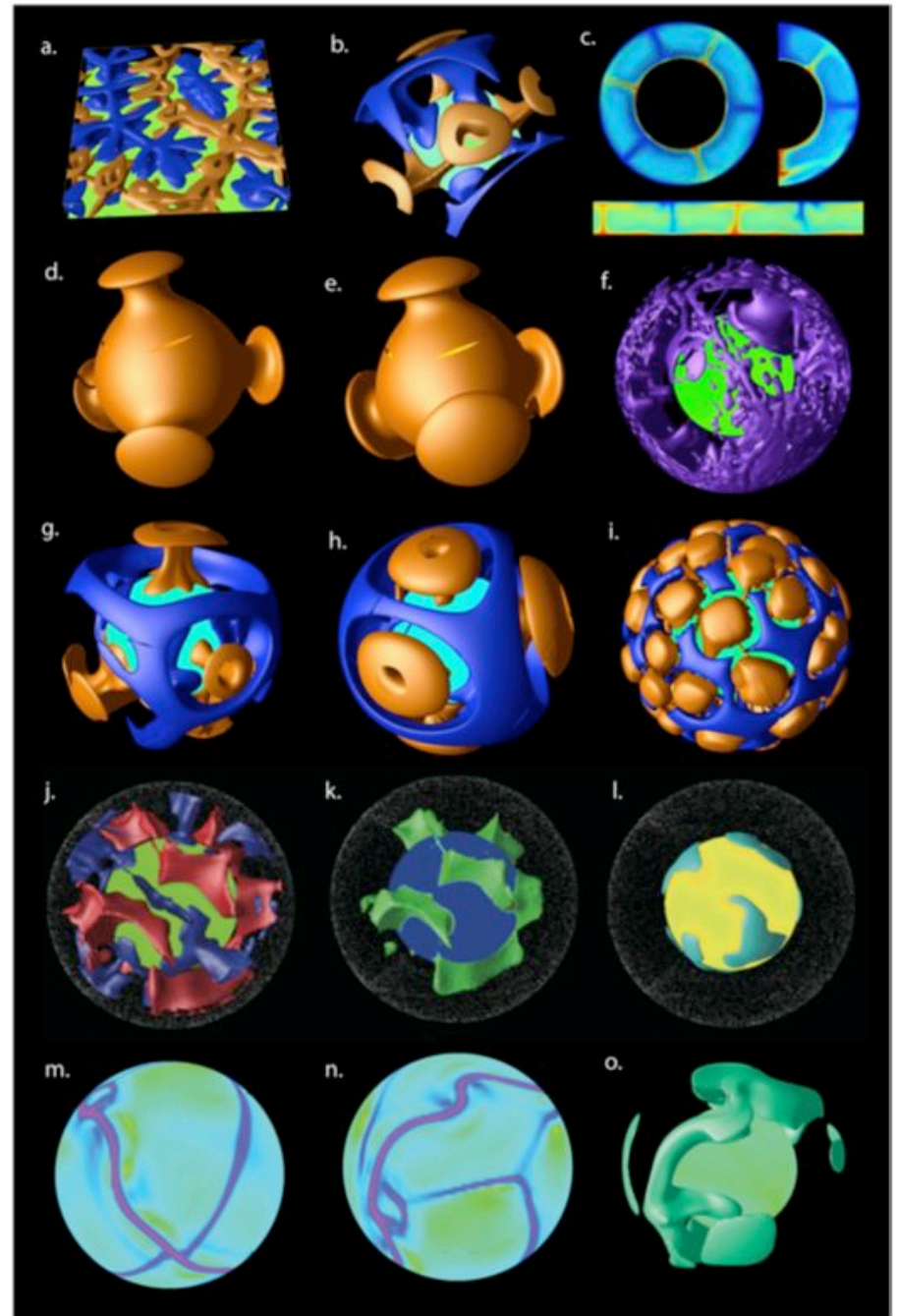
Fast +5%



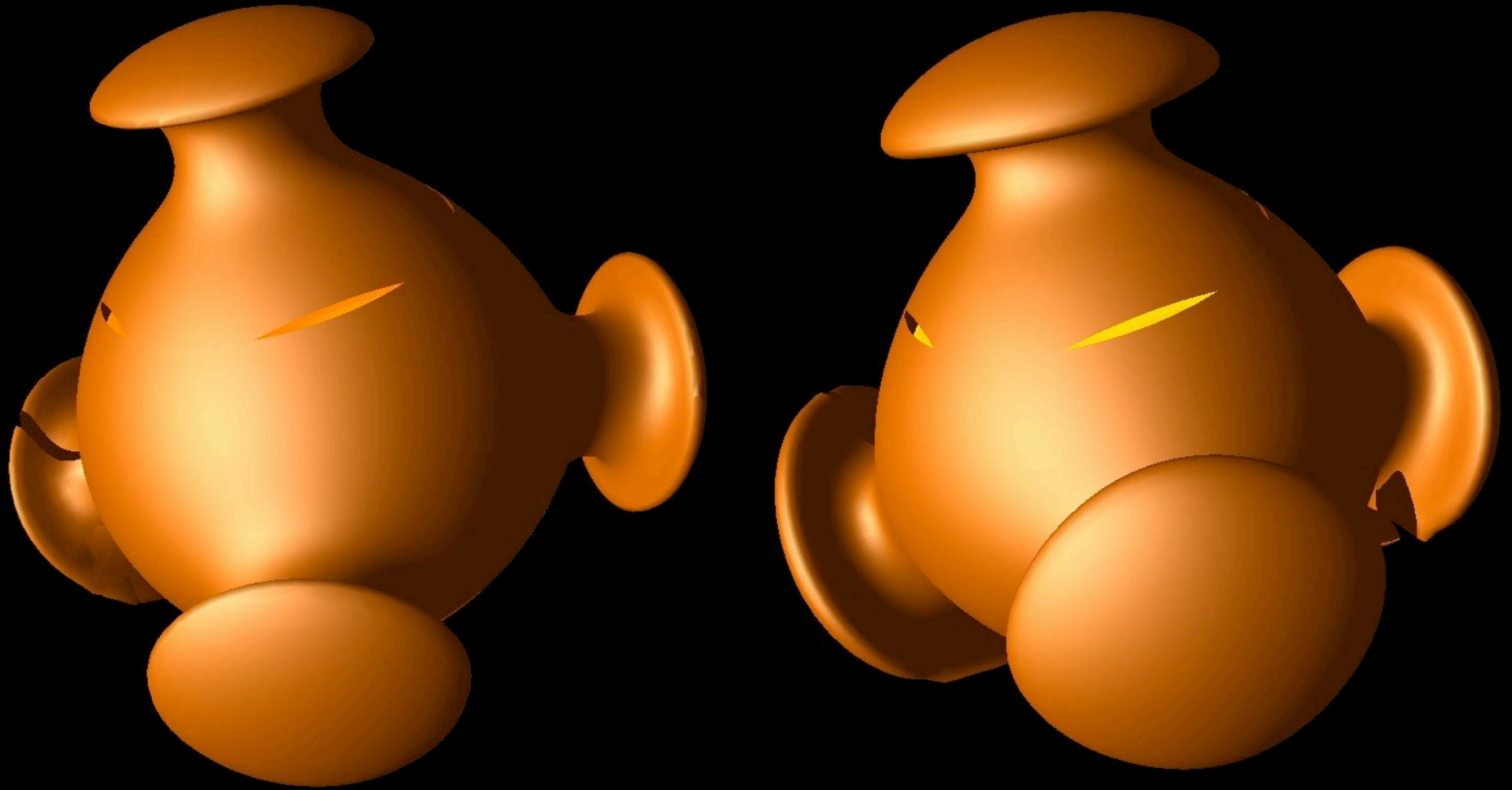
Slow

Using PERPLEX sensitivity

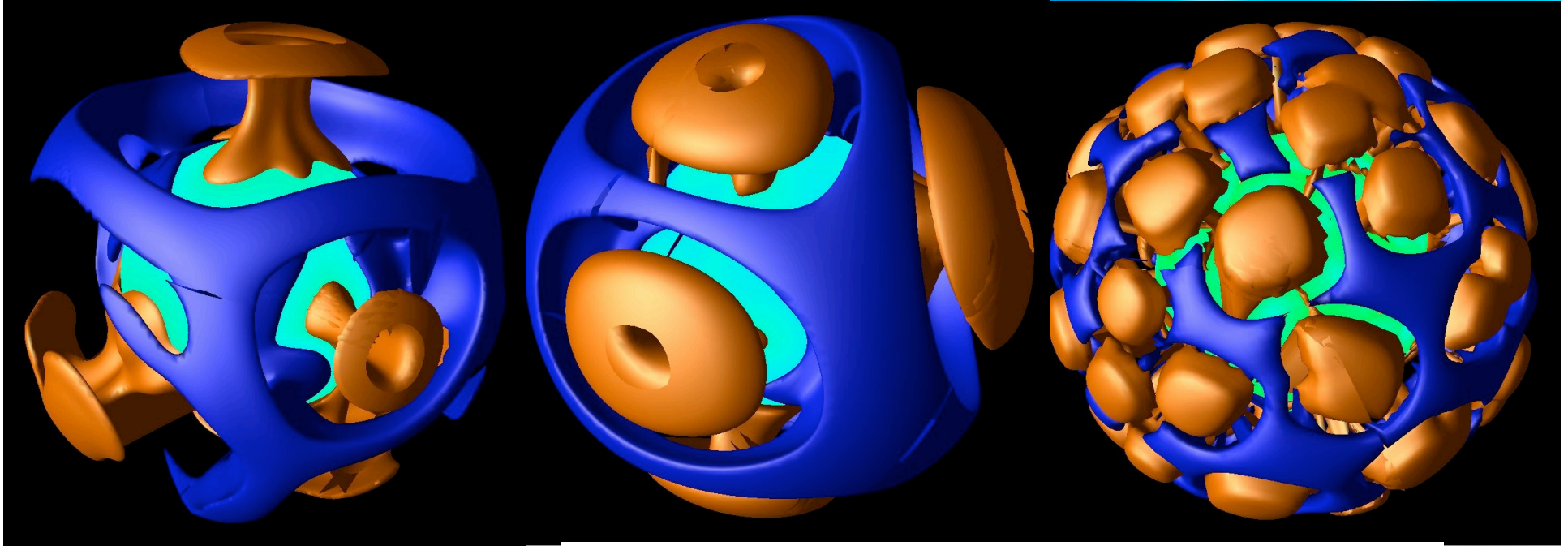
# Examples of applications



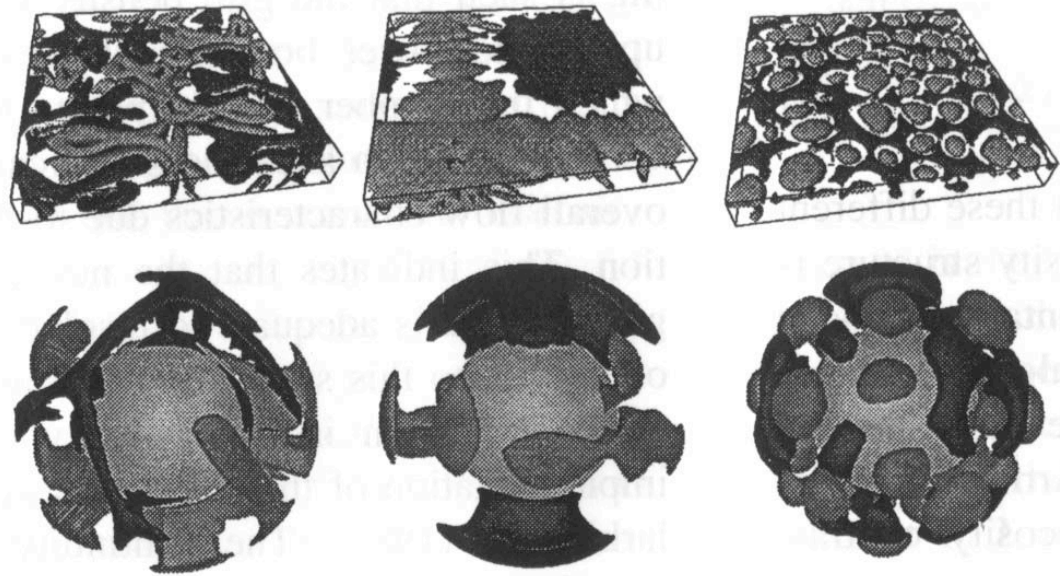
# The usual benchmark tests



# Transitions mobile->sluggish->stagnant lid



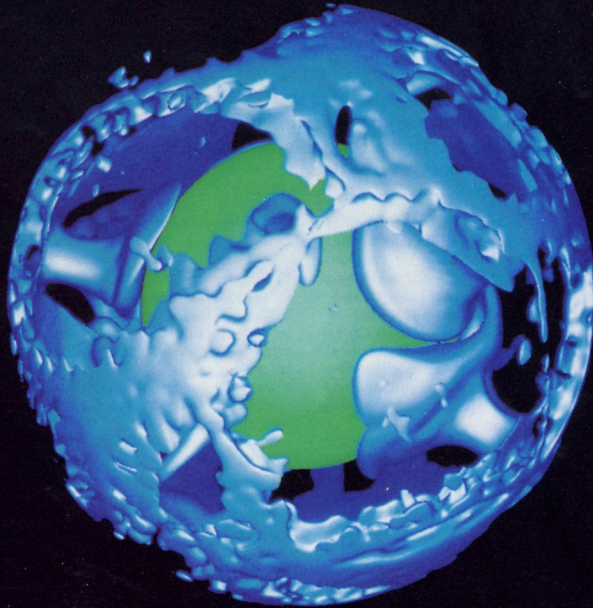
like Ratcliff et al 1996



# nature

INTERNATIONAL WEEKLY JOURNAL OF SCIENCE

Volume 361 No. 6414 25 February 1993 \$7.75

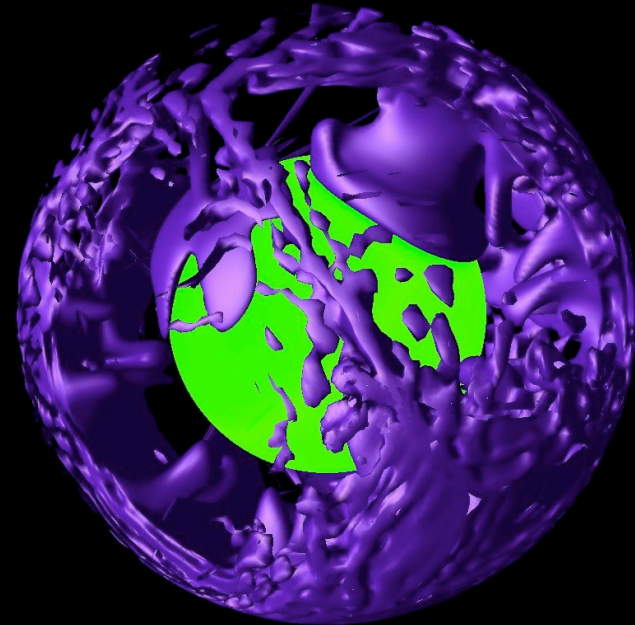


## Avalanches in the mantle

1993: supercomputer,  
spectral code

Biotechnology  
PRODUCT REVIEW

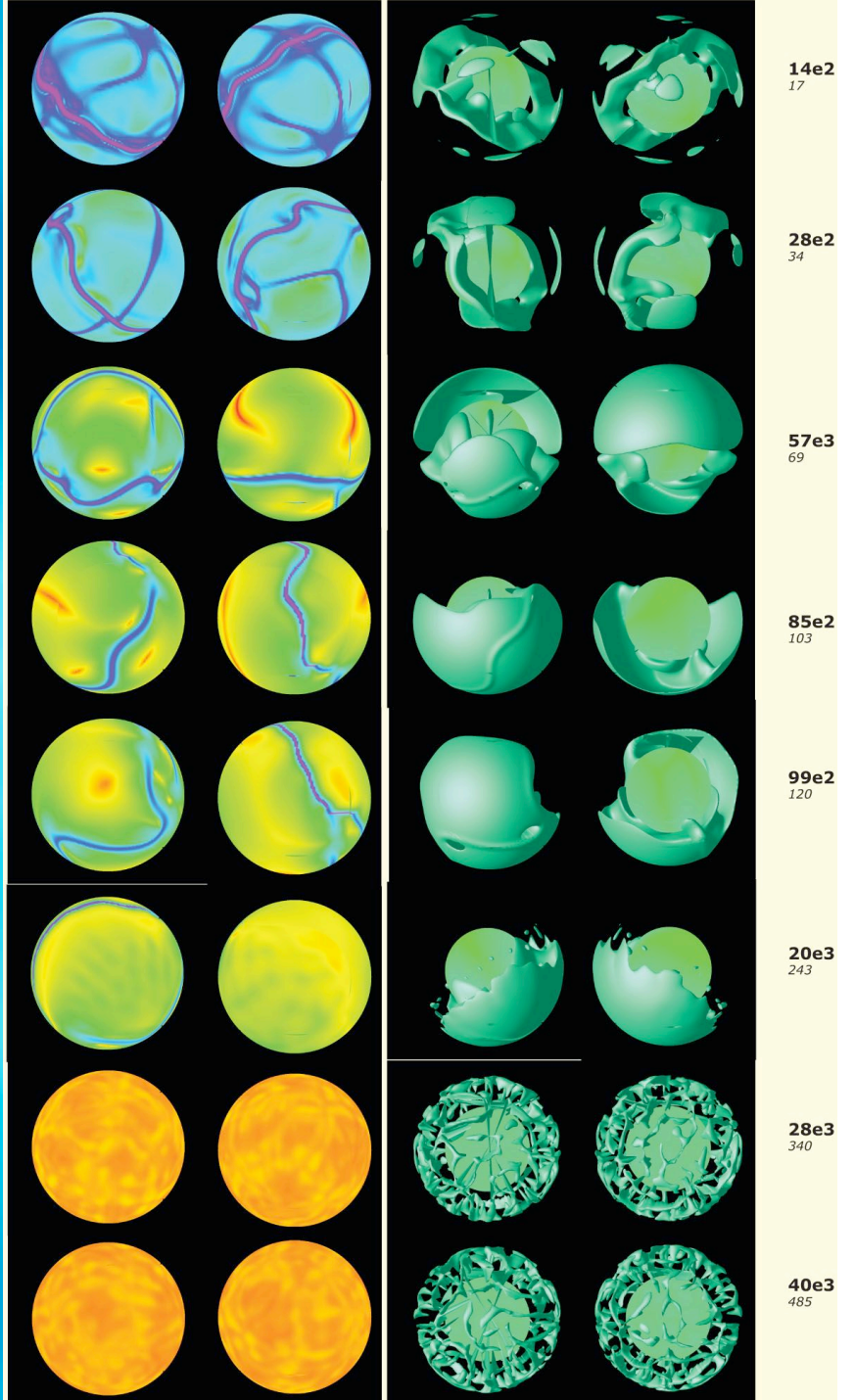
15 years of progress



2008: laptop,  
multigrid code

# Generation of plate tectonics

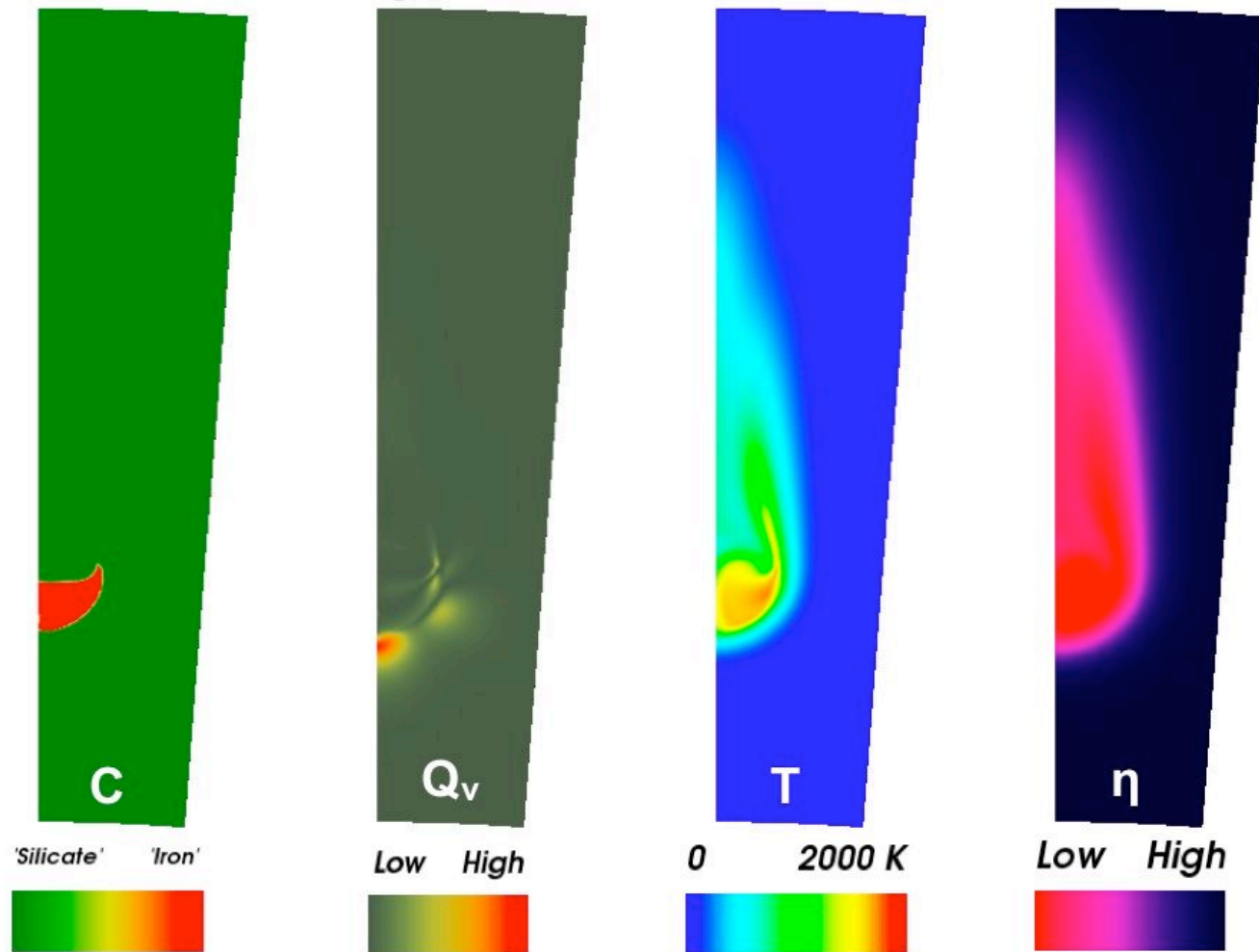
Hein van Heck & me,  
submitted to GRL



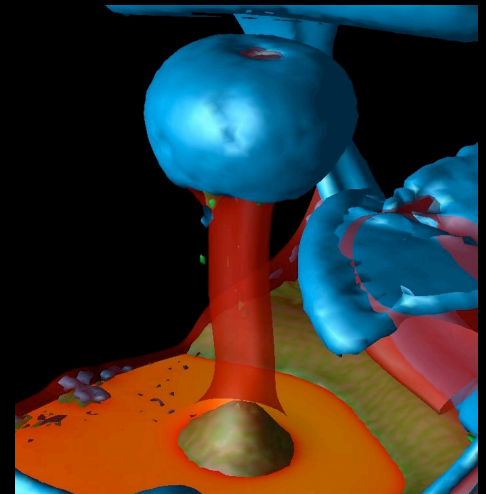
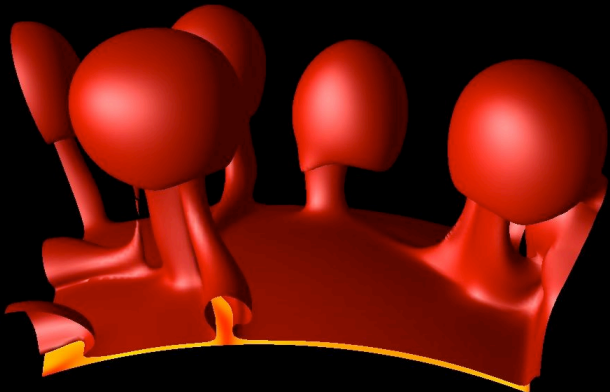
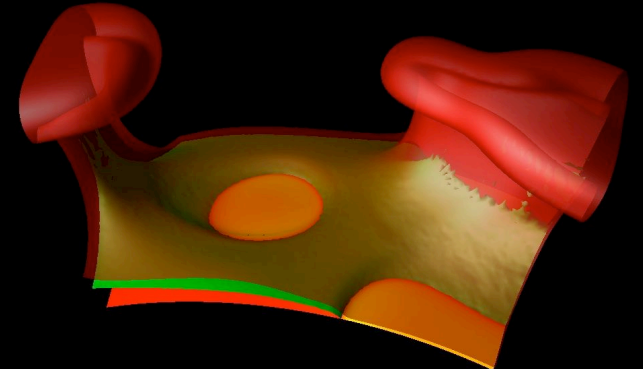
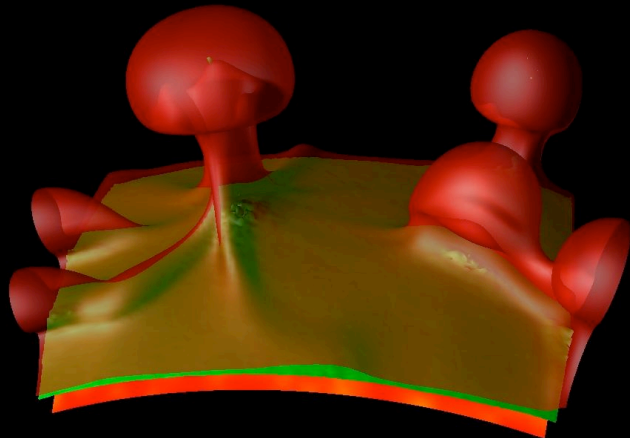
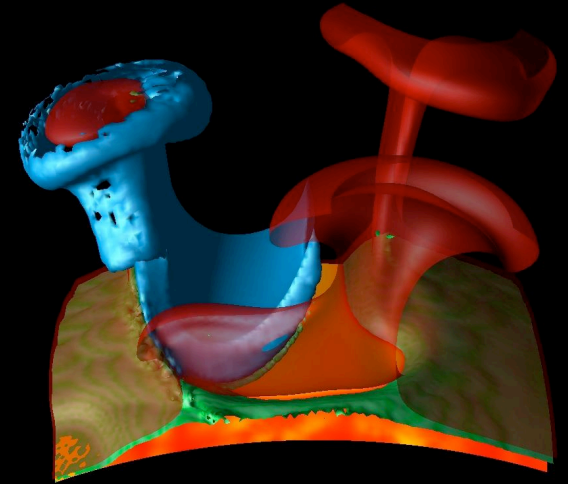
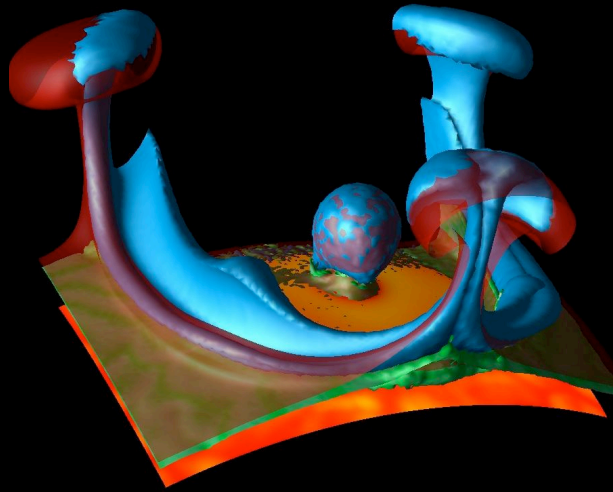
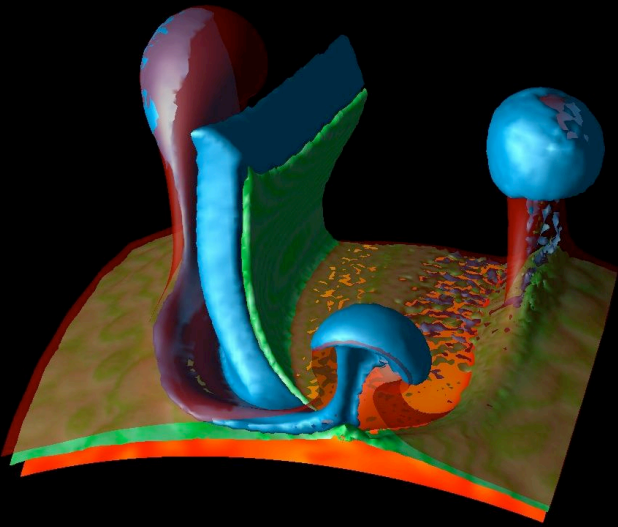




# Henri Samuel: Core formation (G3, 2008)



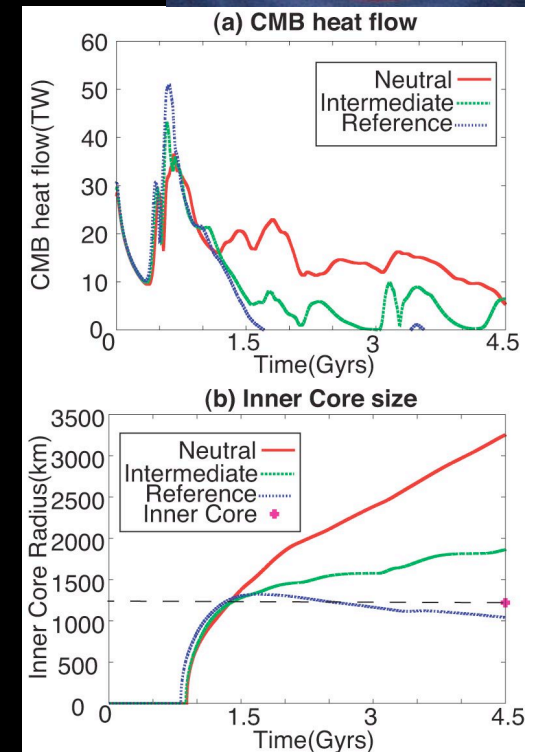
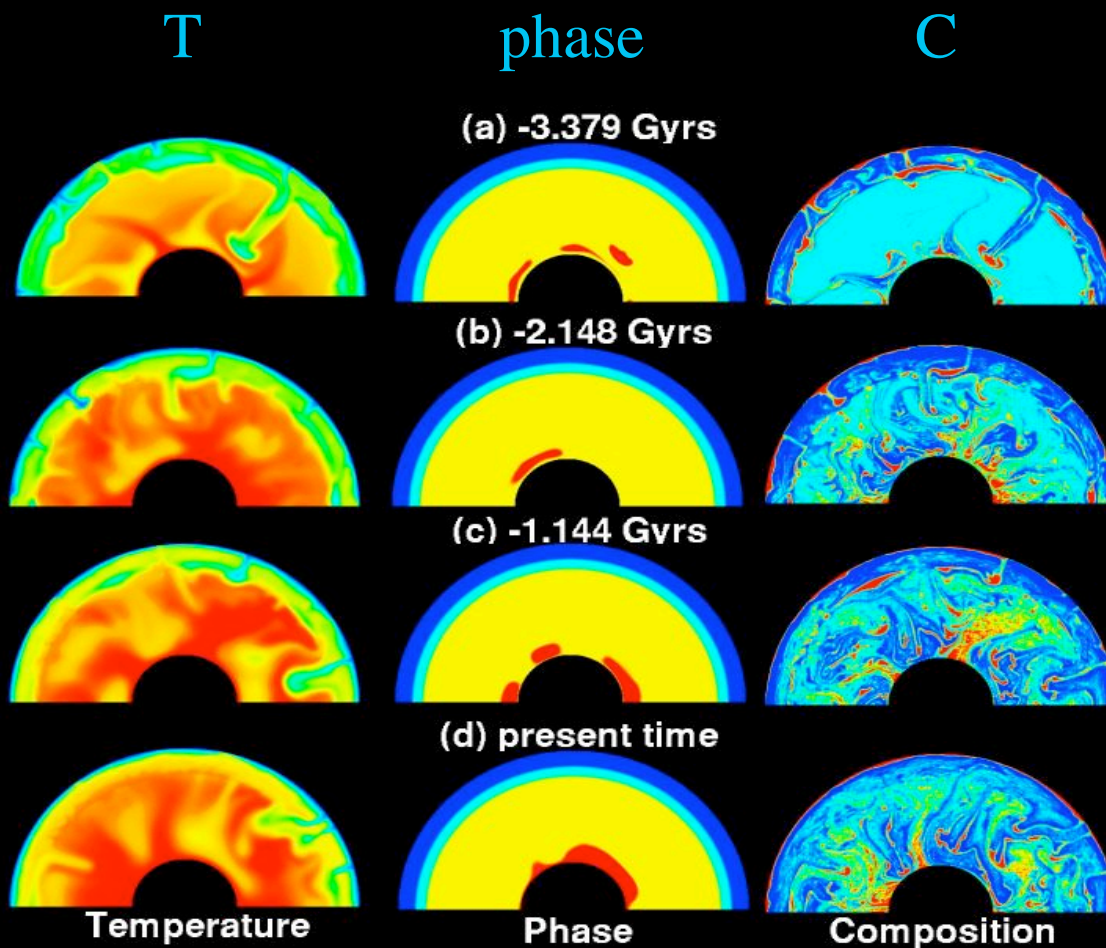
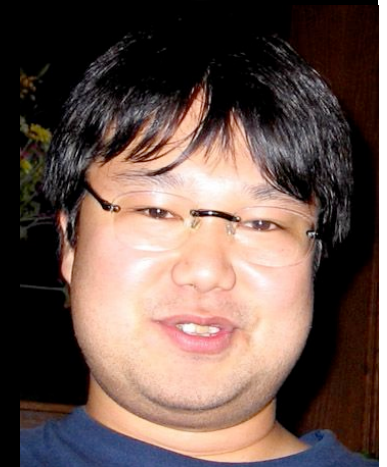
Slab-CMB  
interaction  
(me)



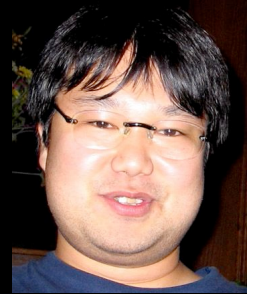
# Thermo-chemical evolution of the mantle

Takashi Nakagawa

## Effect of PPV phase transition Coupled core-mantle evolution



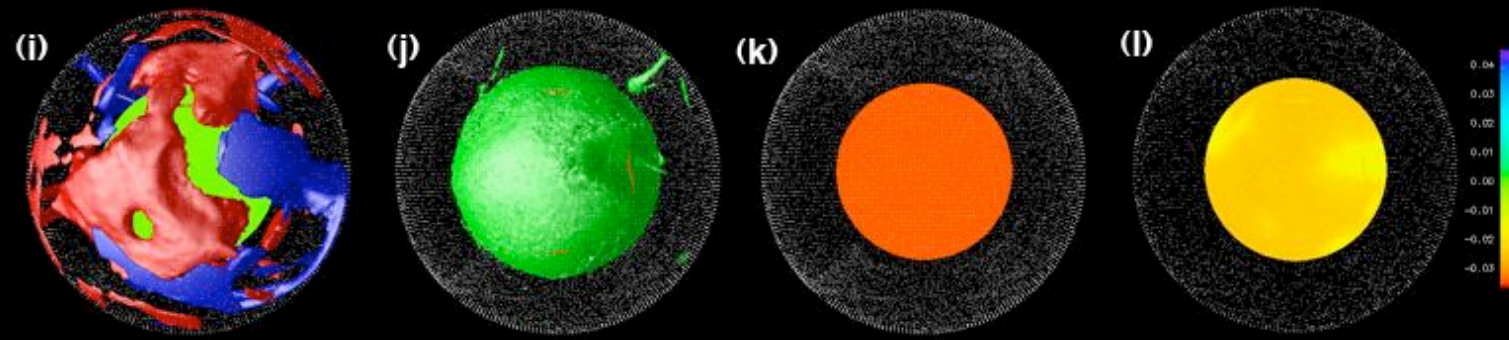
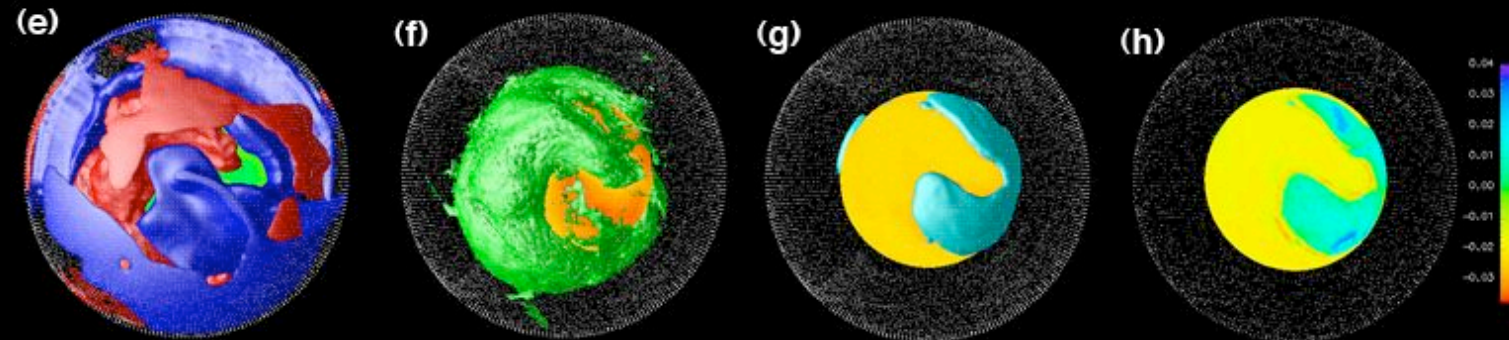
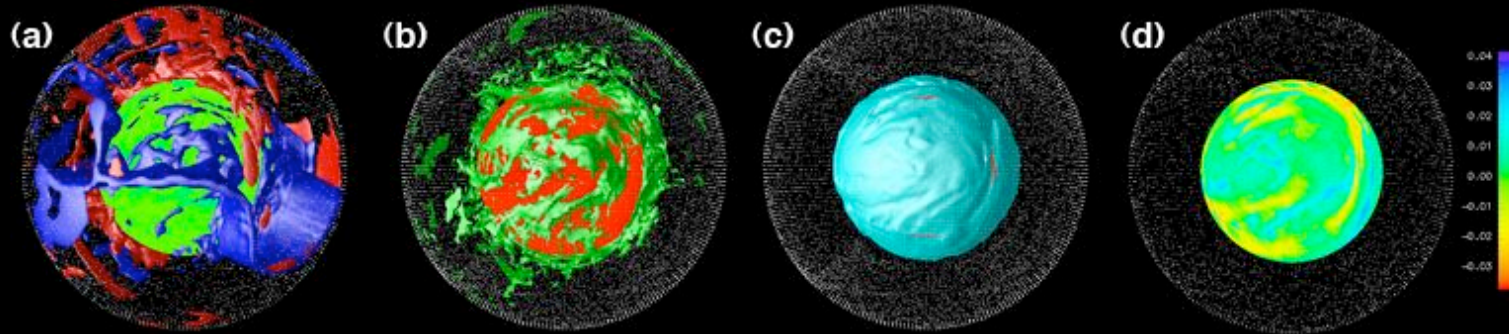
# Spherical results



0.0%

1.8%

3.6%



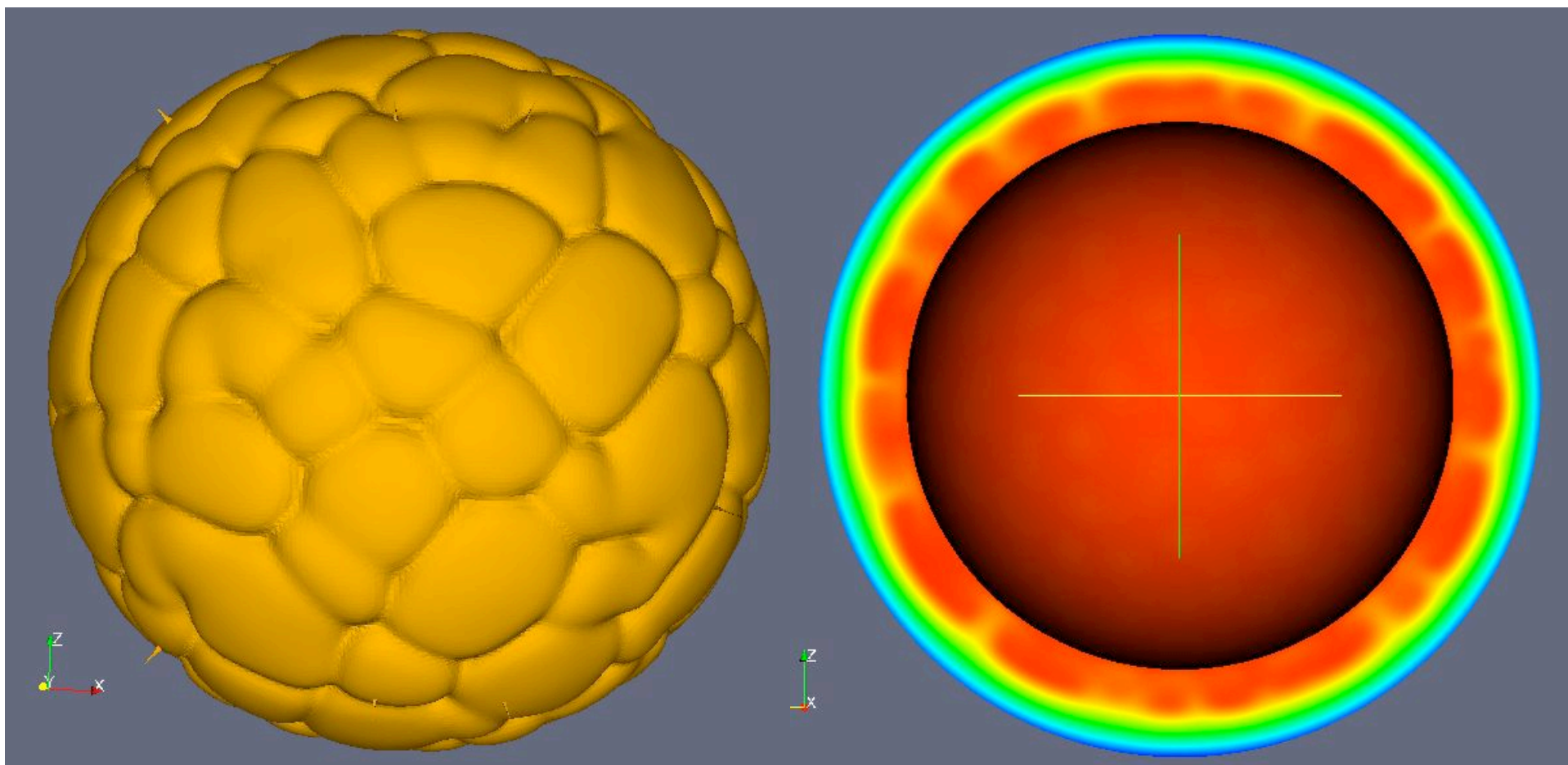
Temp.

Comp.

PPV

S-anomalies

# Mercury



# Summary of StagYY

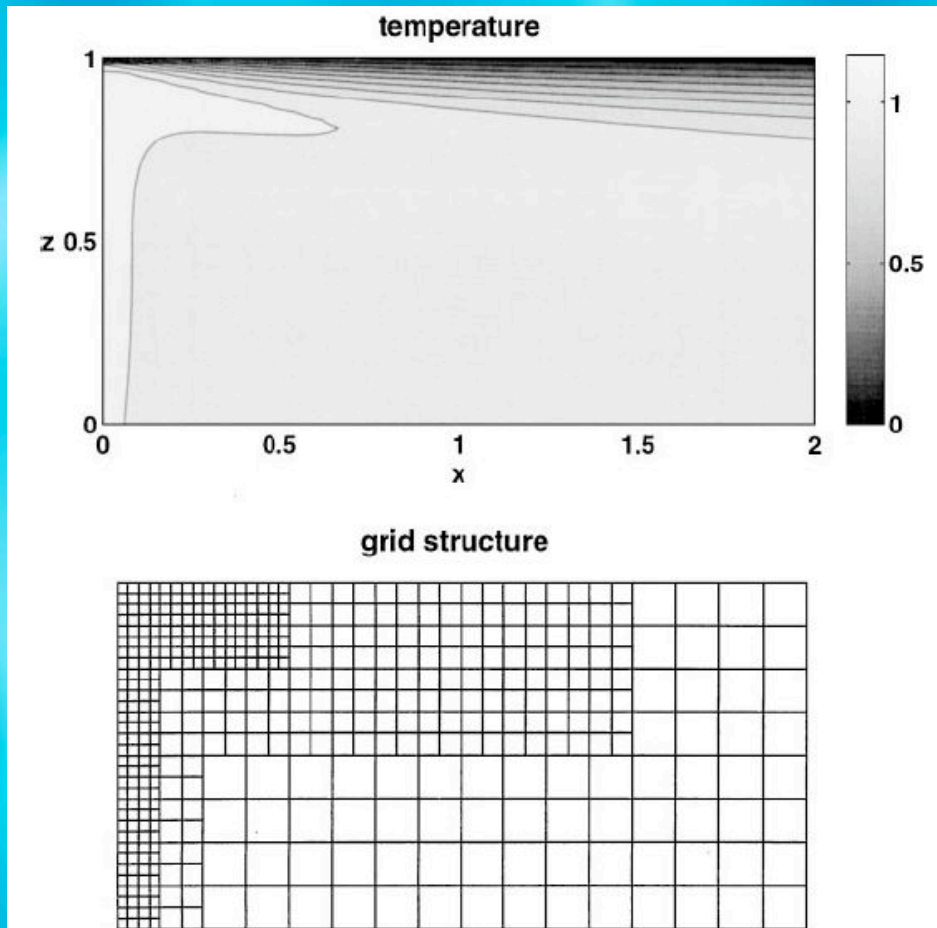
- ⦿ Many geometries including spherical shell using the yin-yang grid
- ⦿ Efficient & scalable multigrid solver, tracers for composition
- ⦿ Large viscosity contrasts due to MDPI
- ⦿ Compressible truncated anelastic
- ⦿ Self-consistent mineralogy
- ⦿ Melting, melt migration, crustal formation
- ⦿ Self-gravitational geoid
- ⦿ Parameterized core cooling
- ⦿ Self-contained – no libraries except MPI

# Future extensions

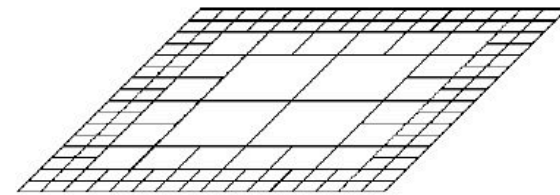
- ◎ Local grid refinement (adaptive?)
- ◎ Visco-elasticity

# Grid refinement

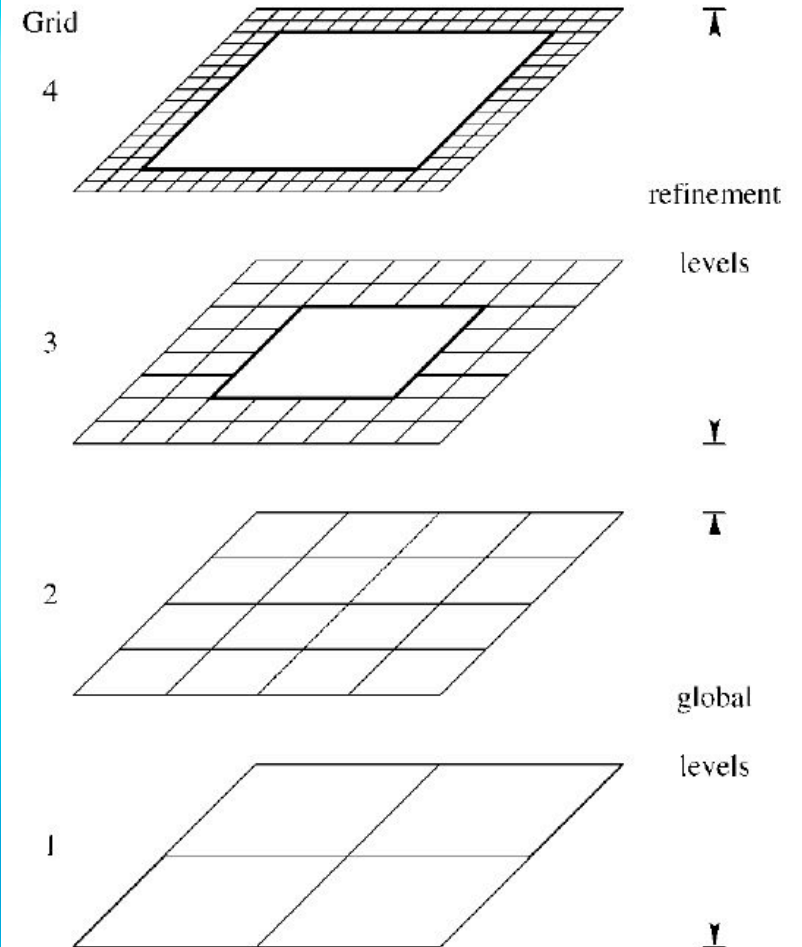
⦿ These figures: Albers



Non-uniform grid



Uniform subgrids





# Using viscous flow solver to treat visco-elasticity

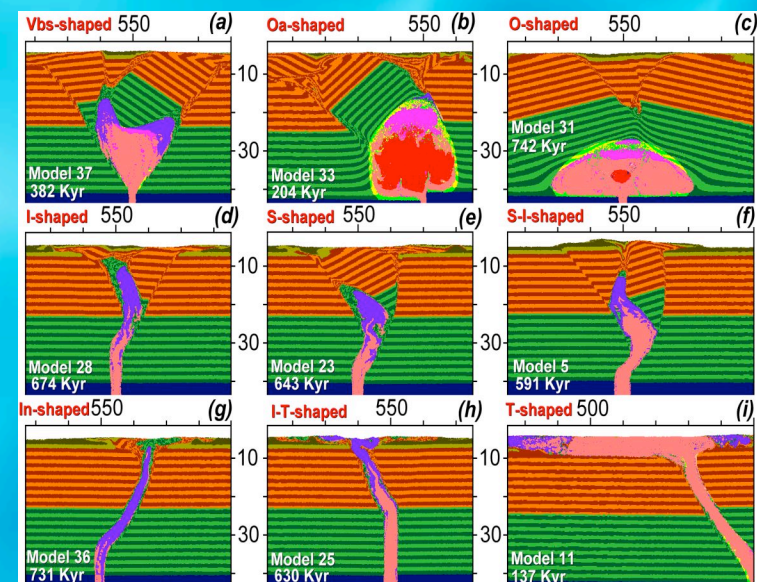
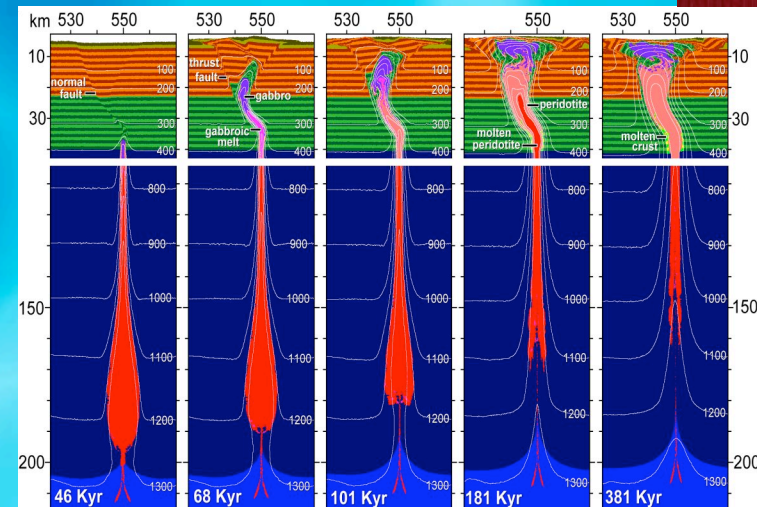
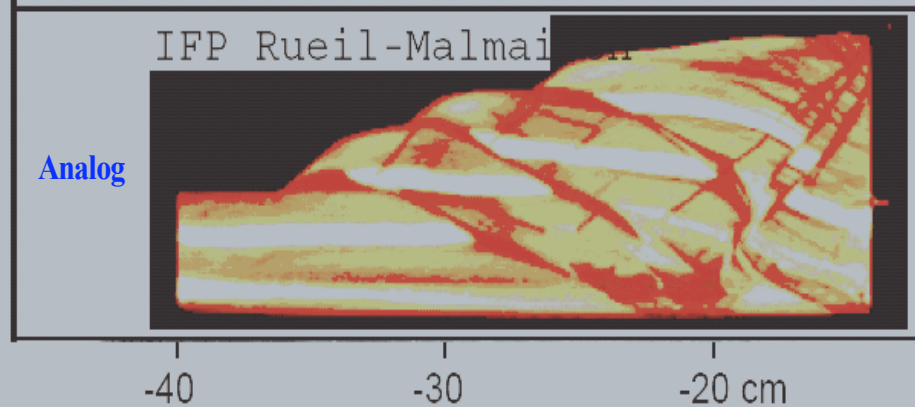
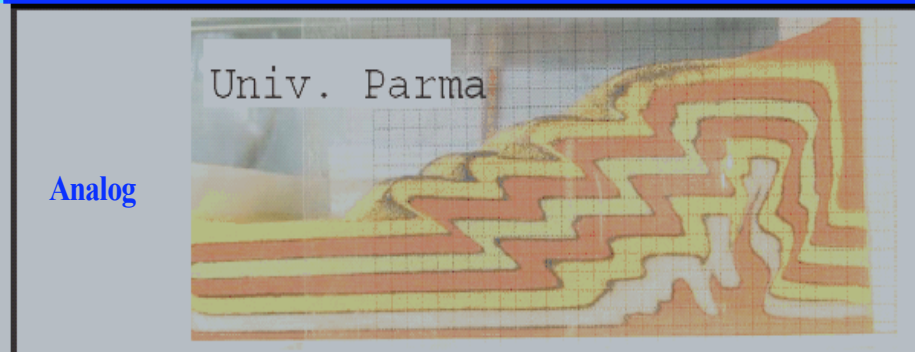
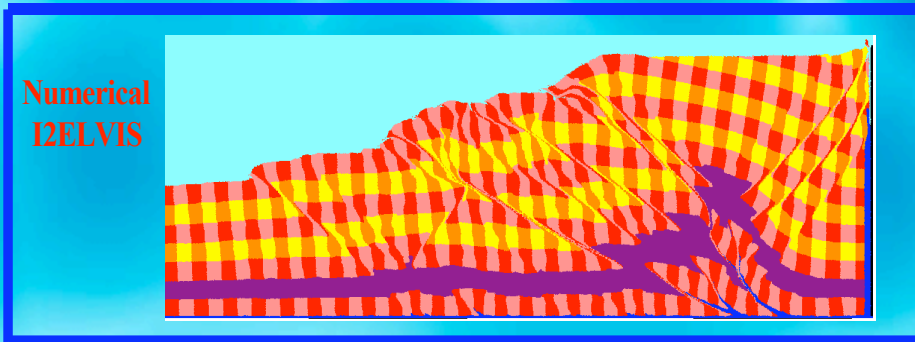
(from Moresi 2002)

$$\eta_{eff} = \eta \frac{\Delta t^e}{\Delta t^e + \alpha}$$

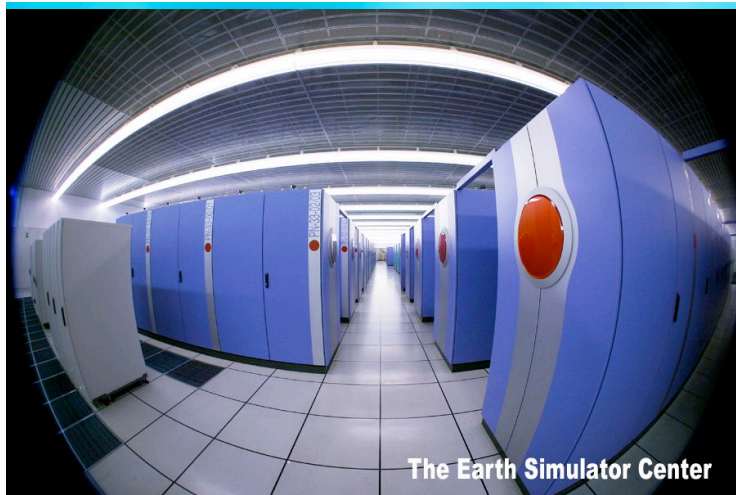
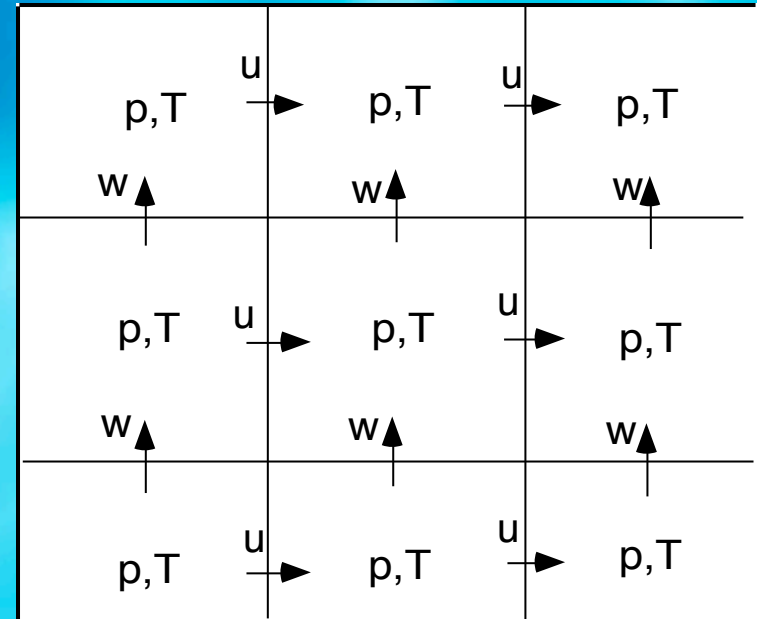
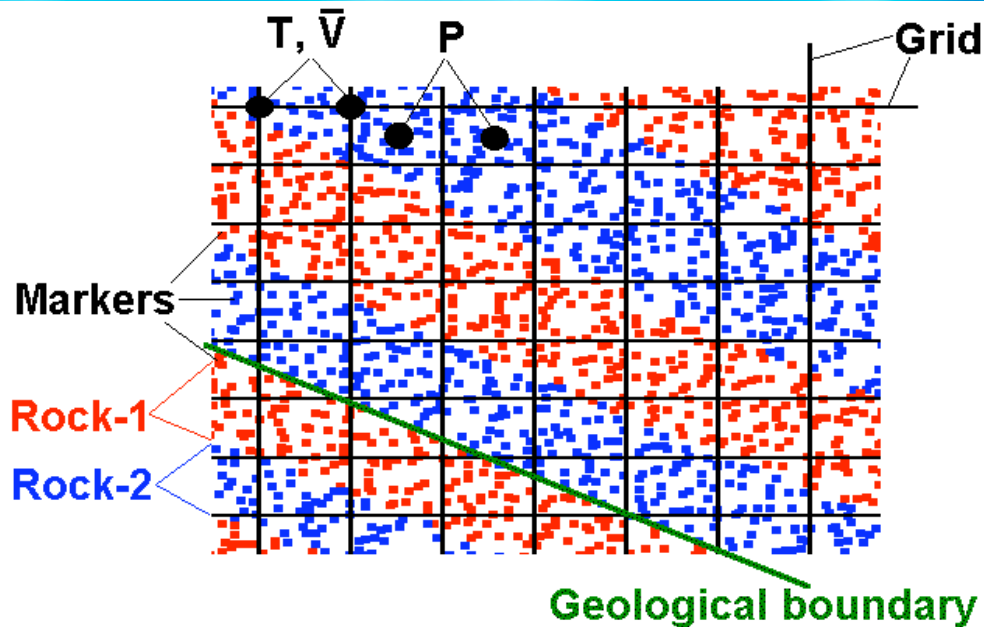
Alpha=relaxation time


$$\boldsymbol{\tau}^{t+\Delta t^e} = \eta_{eff} \left( 2\hat{\mathbf{D}}^{t+\Delta t^e} + \frac{\boldsymbol{\tau}^t}{\mu\Delta t^e} + \frac{\mathbf{W}^t \boldsymbol{\tau}^t}{\mu} - \frac{\boldsymbol{\tau}^t \mathbf{W}^t}{\mu} \right)$$

# Examples: 2D Crustal shortening and magma pipe intrusion (Taras Gerya, ETH, and coworkers)



# Staggered grid finite-differences + marker in cell: solve anything?





**THE END!**